Electronic Supplementary Information

Reactivity of Fluorographene is Triggered by Point Defects: Beyond the Perfect 2D World

Miroslav Medveď,[†,*] Giorgio Zoppellaro,[†] Juri Ugolotti,[†] Dagmar Matochová,[†] Petr Lazar,[†]
Tomáš Pospíšil,[‡] Aristides Bakandritsos,[†] Jiří Tuček,[†] Radek Zbořil,[†] Michal Otyepka[†,*]

[†] Regional Centre of Advanced Technologies and Materials, Department of Physical Chemistry, Faculty of Science, Palacky University in Olomouc, 17. listopadu 1192/12, 771 46 Olomouc, Czech Republic

[‡] Centre of the Region Haná for Biotechnological and Agricultural Research, Department of Chemical Biology and Genetics, Faculty of Science, Palacky University in Olomouc, 17. listopadu 1192/12, 771 46 Olomouc, Czech Republic

Contents

1 Experimental measurements

1.1 EPR measurements of GrF in benzene and DMF

Concentrated suspensions of graphite fluoride (GrF, $C_1F_{1.1}$) (15 mg GF/ mL solvent) were mechanically stirred at 40 °C without sonication in air tight and oxygen-free vials, and EPR spectra of the dense suspensions were recorded over a 10 days frame-period. EPR spectra were recorded on JEOL JES-X-320 operating at X-band frequency (~9.14-.17 GHz), equipped with a variable temperature control ES 13060DVT5 apparatus. The cavity Q quality factor was kept above 6000 in all measurements and signal saturation was avoided by working at low-applied microwave power except in the cases where the power saturation behavior was studied. 0.1 mL of GrF suspensions were usually loaded onto the EPR tubes by using air-tight syringes, or in the case of GrF powder, 10 mg. Highly-pure quartz tubes were employed (Suprasil, Wilmad, ≤ 0.5 OD). Simulation of the EPR traces were carried out by the WinEPR SimFonia software (V.1.25, *EPR Division*, Bruker Instruments, Inc., Billerica, USA) using second-order perturbation theory according to the following Hamiltonian:

Solution spectra: $H = g\ \mu_B\ B_0\ S + a\ S.I + g_n\ \mu_N\ B_0\ I$

Powder spectra: $H = \mu_B\ B_0.\mathbf{g}.\mathbf{S} + \mathbf{S.D.S} + \mathbf{S.A.I} + \mathbf{I.P.I} + \mu_N\ B_0.\mathbf{g_n}.\mathbf{I}$

Let us underline that sonication can create radicals due to cleavage of bonds, as noted in section 5 of the main manuscript. Therefore, EPR studies on solvent induced radical formation on the carbon skeleton would be irrelevant for sonicated samples. As a result, such studies on fluorographene sheets produced through sonication would be misleading. Despite this limitation, it should be stressed that the original radical centers in GrF studied by EPR are point defects restricted inside the 2D atomically thin graphene sheets. This is valid whether the individual sheets are packed together in the 3D non-covalent GrF crystal, or are freely floating in the medium. Furthermore, the solvent-induced radical formation is naturally restricted to the surface-exposed 2D sheets, since the rest sheets in the bulk material are hidden bellow the exposed ones, and do not come in contact with the solvent. The system somehow self-restricts the studies on the atomically thin interface between the exposed sheets and the solvent, rather than between the 3D GrF crystal with the solvent. In conclusion, despite the use of GrF, rather than FG, the results and conclusions on reactivity of FG drawn from the EPR studies performed under the reported procedures remain fully valid.

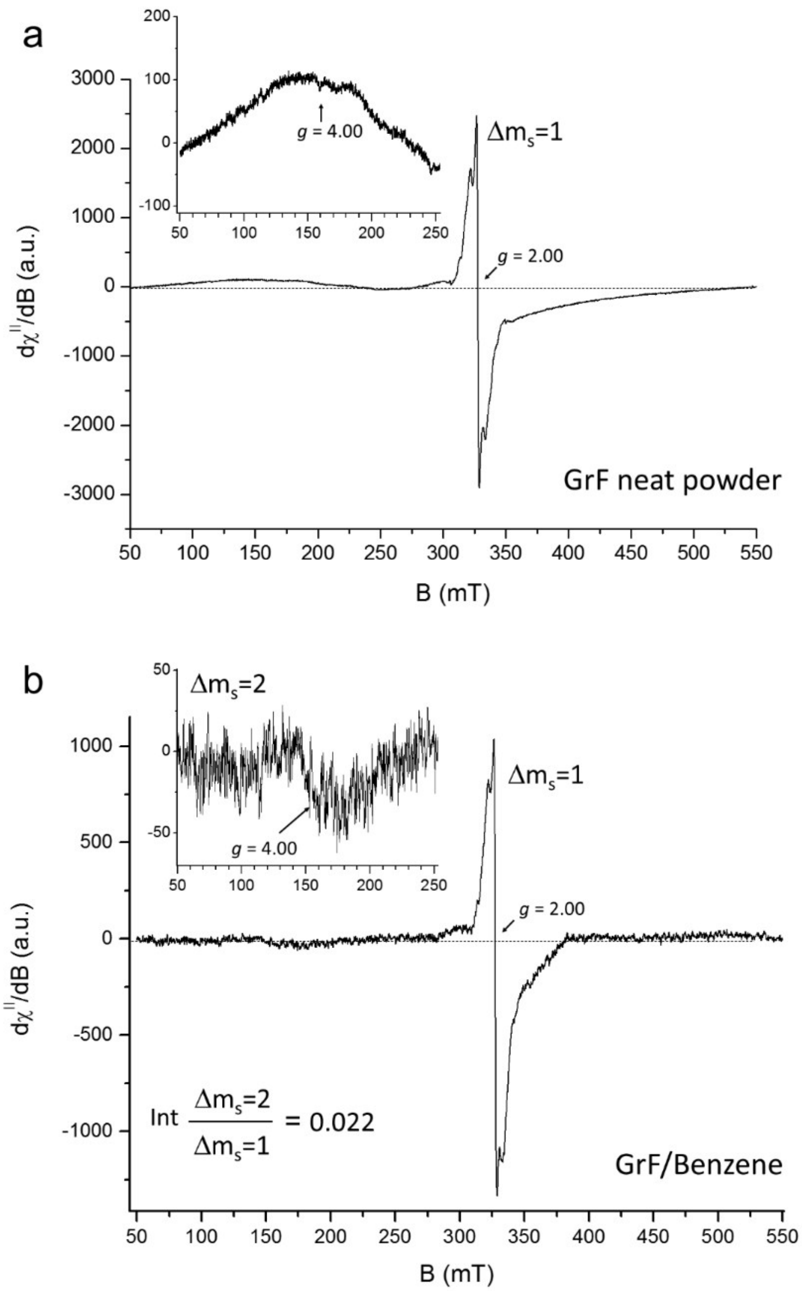

Figure S1 **(a)** X-band EPR spectrum of GrF (neat solid, commercial GrF powder ($(CF_x)_n$, x~1.1, CAS number: 51311-17-2) and **(b)** GrF dispersed in benzene recorded at 143 K **(a)** and 133 K **(b)**. Experimental parameters: **(a)** 9.153187 GHz, 100.00 kHz mod. frequency, 0.8 mT mod. width, time const. 0.03 s, sweep time 4 min, microwave power 1.0 mW, 1 scan. **(b)** 9.145559 GHz, 100.00 kHz mod. frequency, 0.8 mT mod. width, time const. 0.03 s, sweep time 4 min, microwave power 4 .0 mW, 40 scan.

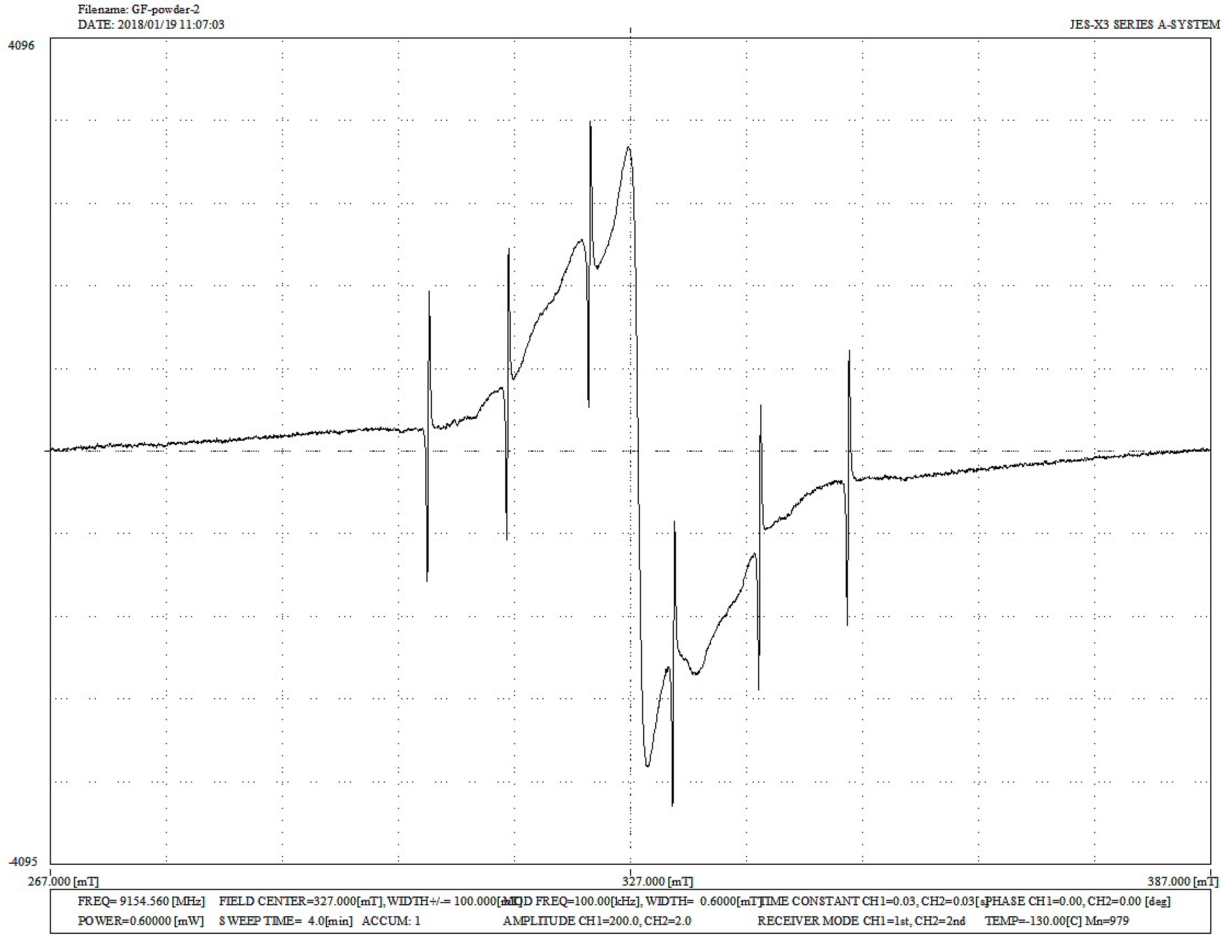

FREQ= 9154.560 [MHz] FIELD CENTER=327.000[mT], WIDTH+/-= 100.000[mT] MOD FREQ=100.00[kHz], WIDTH= 0.6000[mT] TIME CONSTANT CH1=0.03, CH2=0.03[s] PHASE CH1=0.00, CH2=0.00 [deg]
POWER=0.60000 [mW] SWEEP TIME= 4.0[min] ACCUM: 1 AMPLITUDE CH1=200.0, CH2=2.0 RECEIVER MODE CH1=1st, CH2=2nd TEMP=-130.00[C] Mn=979

Figure S2 X-band EPR spectrum of GrF (neat solid) recorded together with Mn(II)MgO standard (JEOL internal reference standard, Mn(II), g_{eff} = 2.00101±0.00005). Experimental parameters: 9.154560 GHz, 100.00 kHz mod. frequency, 0.6 mT mod. width, time const. 0.03 s, sweep time 4 min, microwave power 0.6 mW, 1 scan, T = 143 K. Estimated g_{eff} of GrF is 1.99876, which has been approximated in the manuscript to g_{eff} = 2.000.

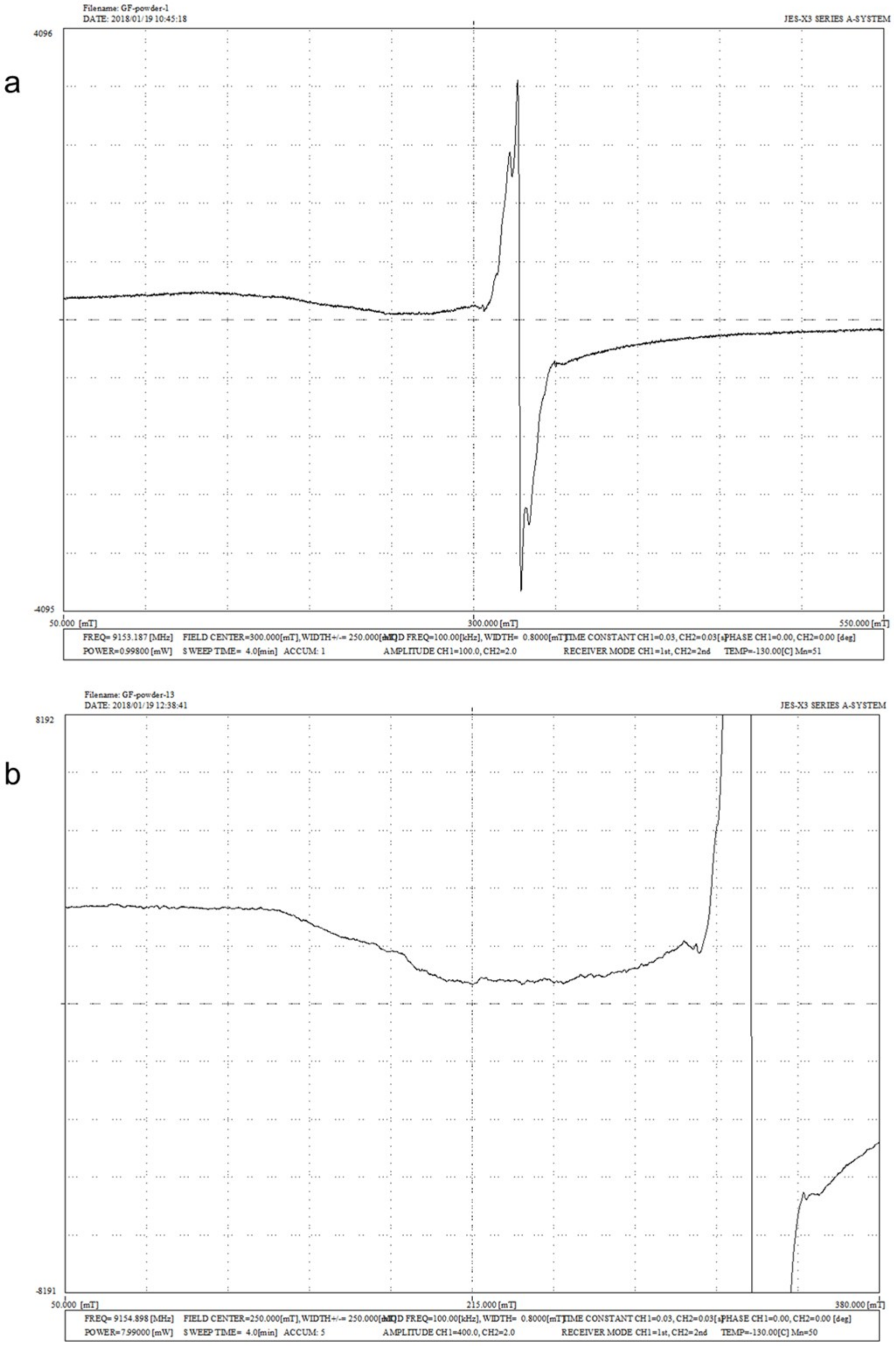

Filename: GF-powder-1
DATE: 2018/01/19 10:45:18
JES-X3 SERIES A-SYSTEM
FREQ= 9153.187 [MHz] FIELD CENTER=300.000[mT], WIDTH+/-= 250.000[mT] MOD FREQ=100.00[kHz], WIDTH= 0.8000[mT] TIME CONSTANT CH1=0.03, CH2=0.03[s] PHASE CH1=0.00, CH2=0.00 [deg]
POWER=0.99800 [mW] SWEEP TIME= 4.0[min] ACCUM: 1 AMPLITUDE CH1=100.0, CH2=2.0 RECEIVER MODE CH1=1st, CH2=2nd TEMP=-130.00[C] Mn=51

Filename: GF-powder-13
DATE: 2018/01/19 12:38:41
JES-X3 SERIES A-SYSTEM
FREQ= 9154.898 [MHz] FIELD CENTER=250.000[mT], WIDTH+/-= 250.000[mT] MOD FREQ=100.00[kHz], WIDTH= 0.8000[mT] TIME CONSTANT CH1=0.03, CH2=0.03[s] PHASE CH1=0.00, CH2=0.00 [deg]
POWER=7.99000 [mW] SWEEP TIME= 4.0[min] ACCUM: 5 AMPLITUDE CH1=400.0, CH2=2.0 RECEIVER MODE CH1=1st, CH2=2nd TEMP=-130.00[C] Mn=50

Figure S3 X-band EPR spectra of GrF (neat solid as provided by Sigma-Aldrich) recorded at 1 mW (**a**, 1 scan) and 8.0 mW (**b**, 5 scan) of microwave power, 0.8 mT modulation width and at *T* = 143 K, showing the clear emergence of a broad low-field signal (**a,b**) and a dispersion-signal tail at high field (**a**). Other experimental parameters are given in the plot. No baseline correction has been applied and the spectra have been plotted as recorded.

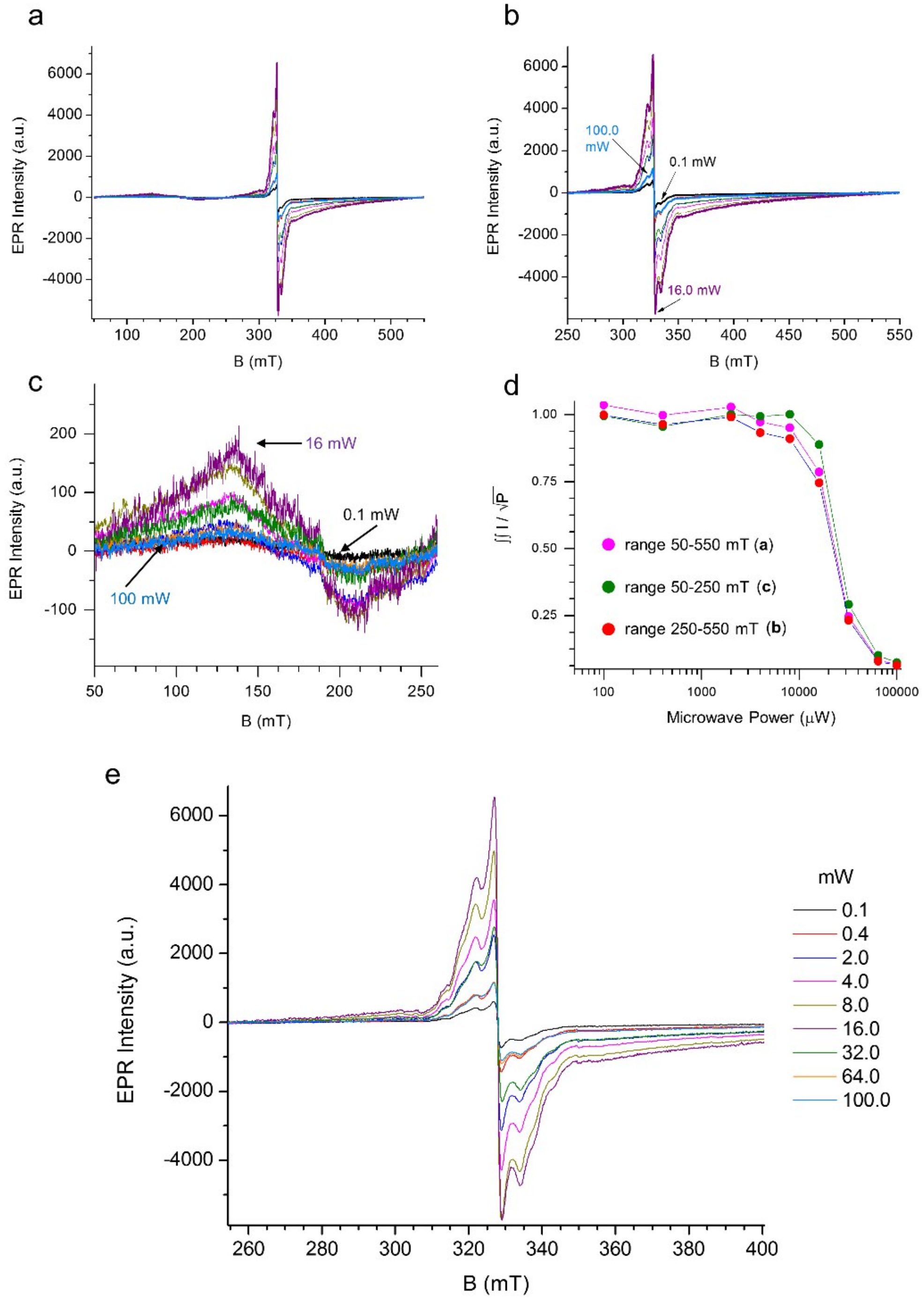

Figure S4 X-band EPR spectra (**a,b,c,e**) of neat GrF solid (powder) recorded under various applied powers at fixed temperature in the magnetic-field range 50-550 mT. Experimental parameters: 9.155073 GHz, 100.00 kHz mod. frequency, 0.6 mT mod. width, time const. 0.03 s, sweep time 4 min, , 1 scan, T = 143 K. Plot **(d)** shows the signal saturation trend, expressed as double integrated signal intensities divided by the square root of the applied powers (∬I/√P) *vs* P (microwave power). The results are derived for the entire sweep-range (corresponding to panel **a**), the high-field range (corresponding to panel **b**) and low field range (corresponding to panel **c**).

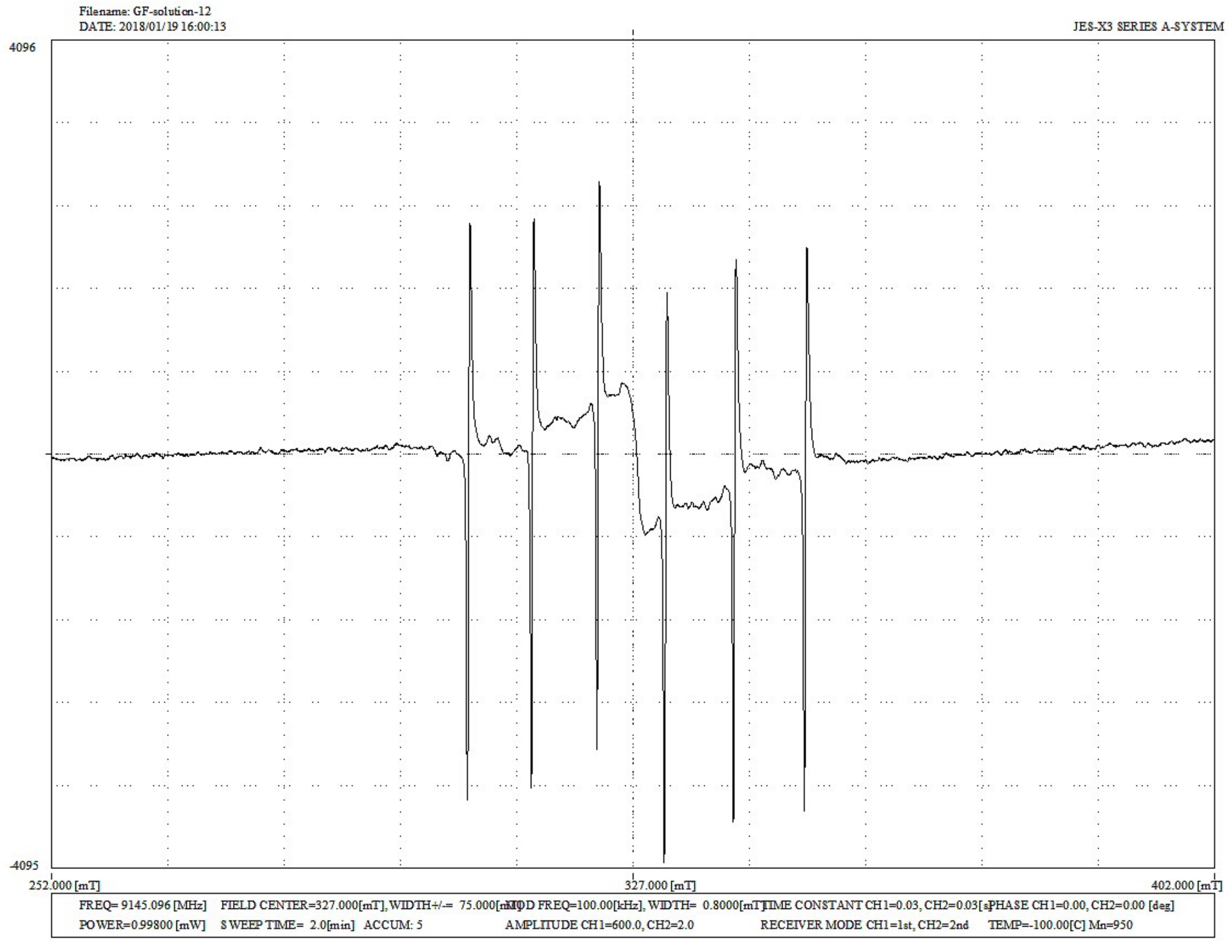

Figure S5. X-band EPR spectrum of GrF/Benzene suspension recorded together with Mn(II)MgO standard (JEOL internal reference standard, Mn(II), g_{eff} = 2.00101±0.00005). Experimental parameters: 9.145096 GHz, 100.00 kHz mod. frequency, 0.8 mT mod. width, time const. 0.03 s, sweep time 2 min, microwave power 0.998 mW, 5 scan, T = 173 K. Estimated g_{eff} of GrF is 1.9996, which has been approximated in the manuscript to g_{eff} = 2.000.

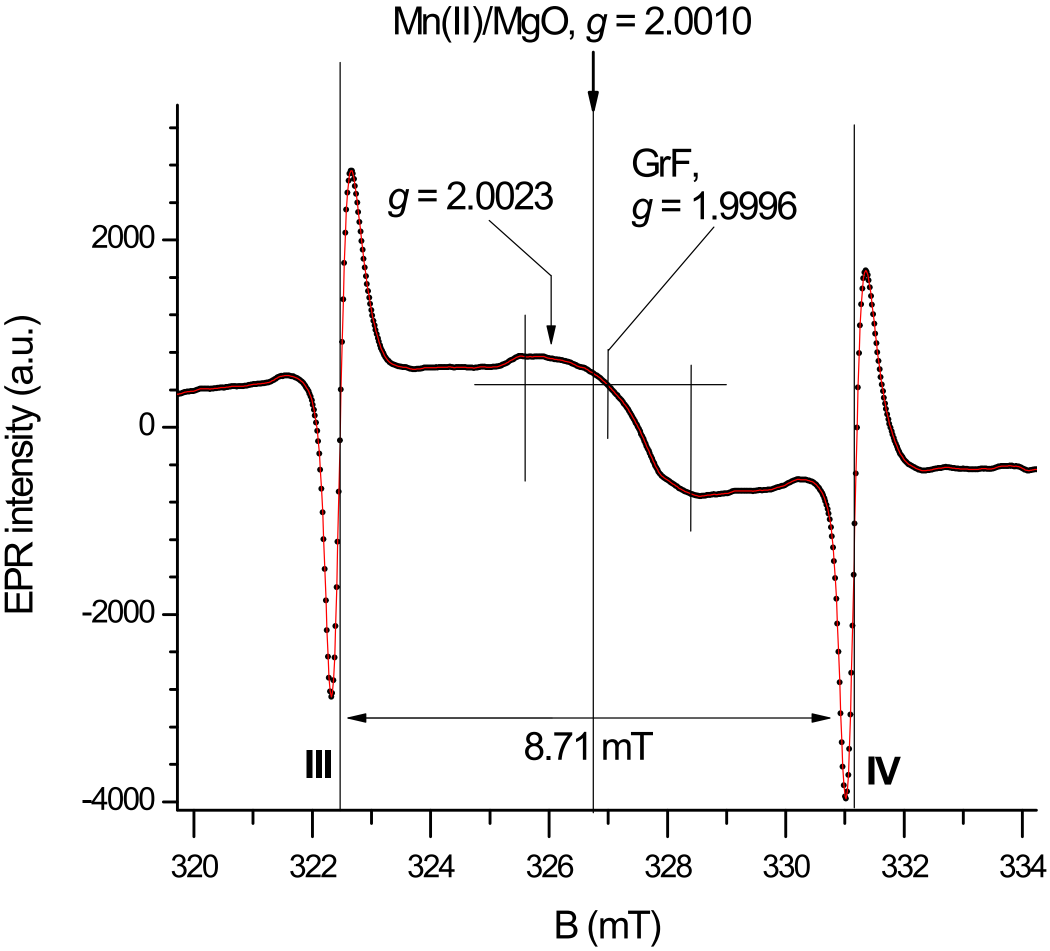

Figure S6 X-band EPR spectrum of GrF/Benzene suspension (frozen-solution) recorded together with Mn(II)MgO standard at 173 K, in the enlarged region from Figure S5. Note that similar results have been obtained for the GrF/DMF suspension.

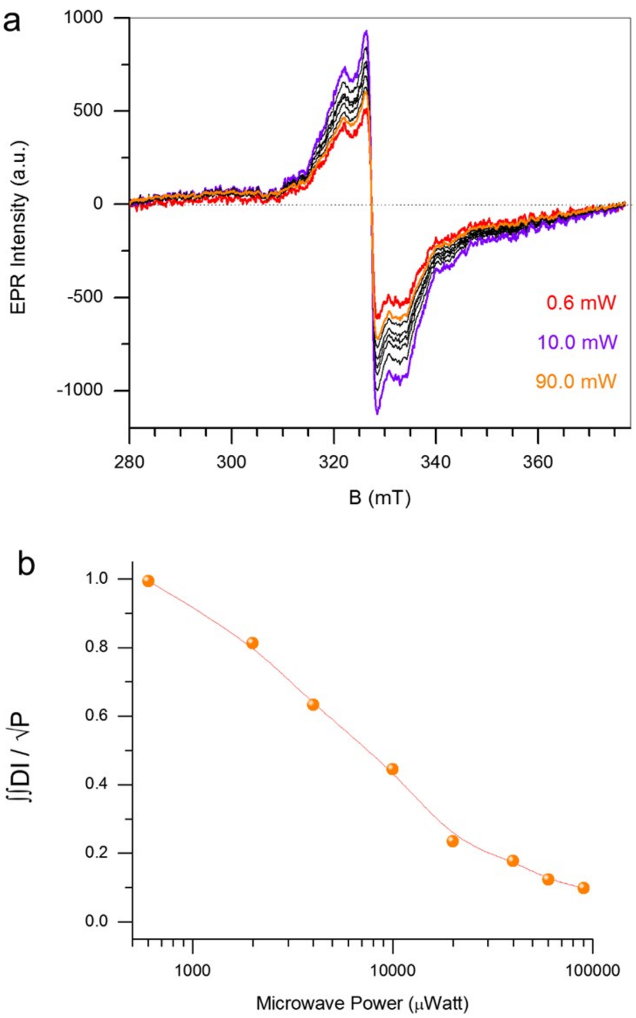

Figure S7 (a) X-band EPR spectra of GrF/Benzene (frozen solution) recorded in function of applied microwave powers at constant temperature around the *g* = 2 region. Experimental parameters: 9.145830 GHz, 100.00 kHz mod. frequency, 0.8 mT mod. width, time const. 0.03 s, sweep time 2 min, , 4 scan, *T* = 133 K. Panel **(b)** shows the saturation plot, expressed as double integrated signal intensities divided by the square root of the applied powers (∫∫I/√P) *vs* P (microwave power).

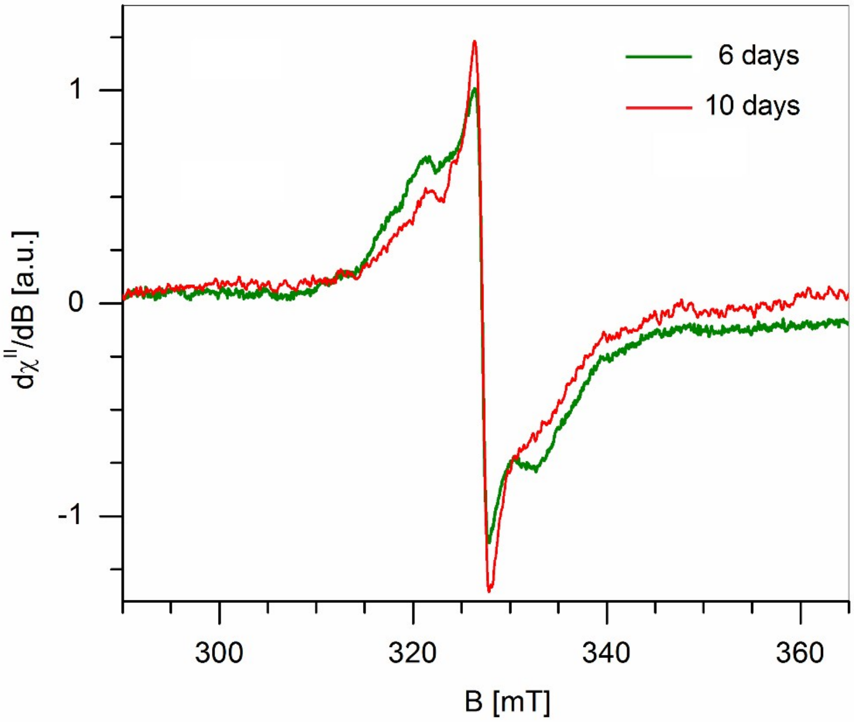

Figure S8 Comparison of the EPR spectra of GrF/Benzene aged for 6 days (green line) and 10 days (red line). Experimental parameters: 9.148212 GHz frequency, 100 kHz modulation frequency, 30 ms time constant, 0.5 mT modulation-width, 0.6 mW of applied microwave power, 4 min sweep-time, *T* of 123 K. 4 scans accumulated and averaged.

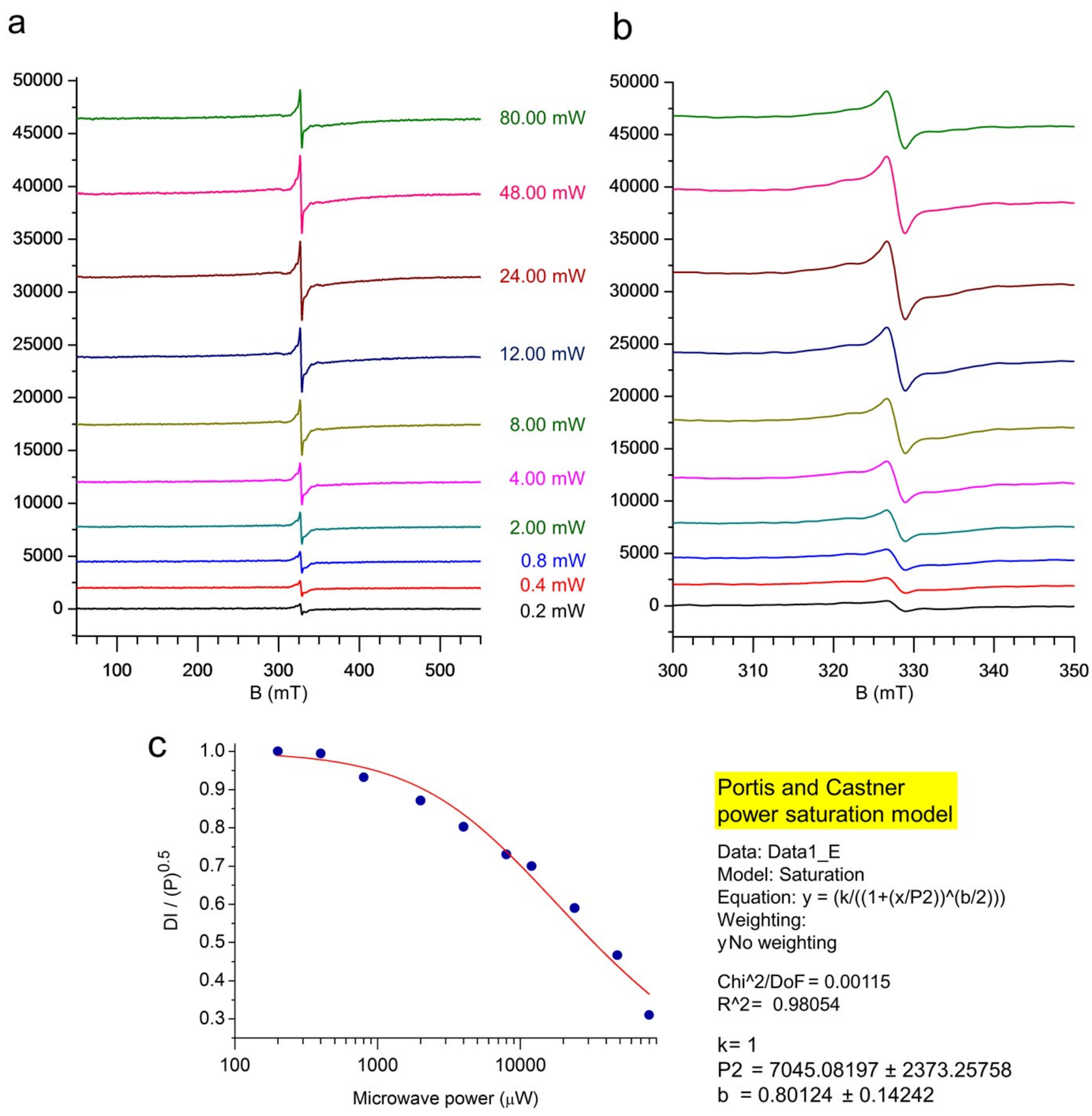

Figure S9 (a,b) X-band EPR spectra of freshly prepared GrF/DMF (frozen solution) recorded in function of the applied microwave power at constant temperature in the broad (50-550 mT) magnetic-sweep region. Spectra were plotted by vertical-shift for easier comparison. Experimental parameters: 9.150947 GHz, 100.00 KHz mod. frequency, 0.7 mT mod. width, time const. 0.03 s, sweep time 4 min, , 2 scan, T = 133 K. Panel **(c)** shows the saturation plot, expressed as double integrated signal intensity in the entire sweep range (50-550 mT) divided by the square root of the applied powers ($DI/P^{0.5}$) *vs* P (microwave power). The red-line is the power-saturation fitting model (Portis[1] and Castner[2]) which provides a relaxation factor *b* that converges to value < 1, suggesting that dipolar and exchange interactions are active in the system.

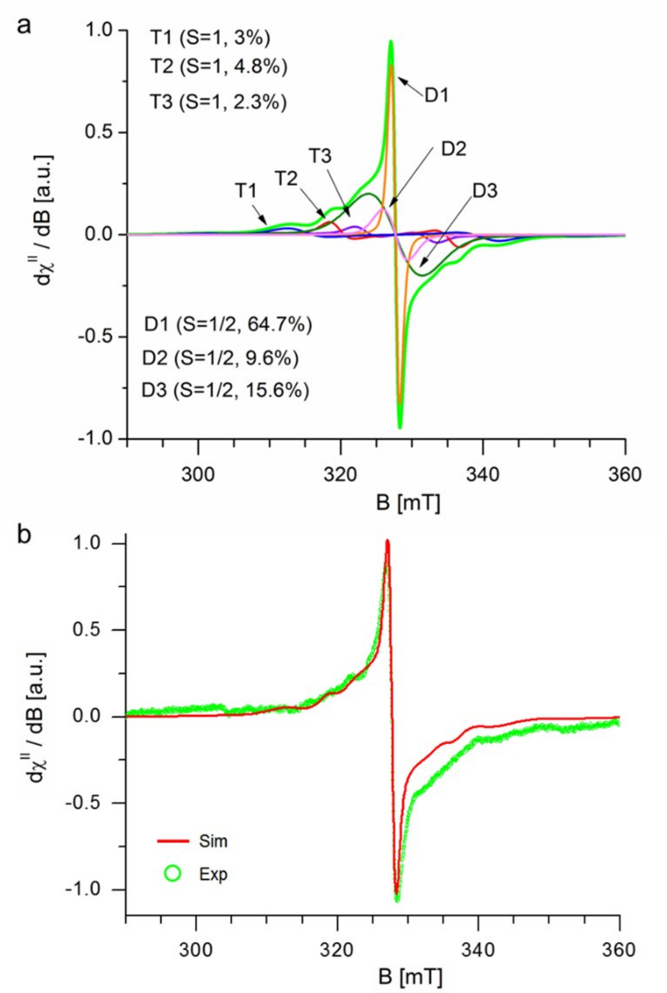

Figure S10 **(a)** Simulation of the X-band (9.17 GHz) EPR resonance line for GrF/DMF in frozen matrix recorded after 6h of stirring (see also main text, Figure 1d) as sum of spin-components, where the labels T1, T2 and T3 indicates the triplet (*S*=1) species. D1, D2 and D3 the doublets (*S*=1/2) species. The relative ratio among the spin components is shown as % (double integrated signal intensity). Spin-Hamiltonian parameters were given in the main text. **(b)** Comparison between the recoded and simulated (from panel a) EPR spectrum in frozen matrix (T = 123 K).

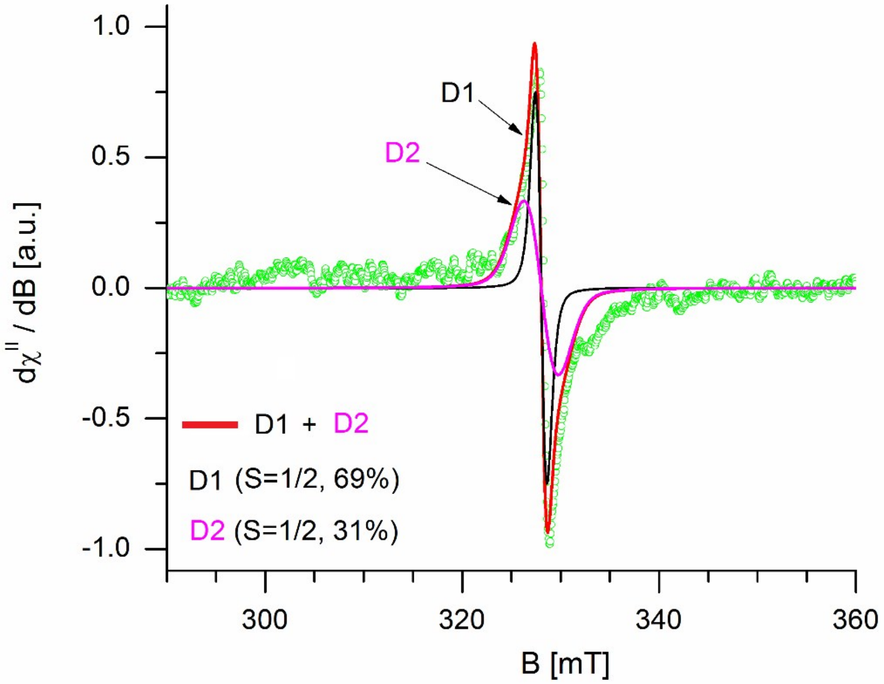

Figure S11 Simulation of the X-band (9.17 GHz) EPR resonance line for GrF/DMF in frozen matrix (T = 123 K) recorded after 10 days of stirring (see main text, Figure 1f) where the labels D1, D2 and are doublets (S=1/2) species. The relative ratio among the spin components is shown as % (total double integrated signal intensity). Spin-Hamiltonian parameters were given in the main text (spin-half components, D1 and D2).

References

1. Portis A.M. *Phys. Rev*. 91, **1953**, 1071-1078.

2. Castner T.J .Jr. *Phys. Rev.* 115, 1**959**, 1506-1515.

1.2 Experimental evaluation of the spin density (Ds)

Spin density (Ds) was evaluated by using the $CuSO_4 \times 5H_2O$ (99.999%, CAS Number: 7758-99-8) as S=1/2 standard and used in powder form. The powder samples (GrF neat powder and 10-days aged in DMF, which was dried in a high vacuum apparatus, were loaded onto polypropylene VSM holders (P125E) (see picture below), and the sealed capsules were put inside an EPR quartz tube. In this way, the same tube, placed at the same high inside the CW-resonator cavity, could be used in all measurements. The measurements were performed at 173 K, with experimental parameters kept identical for standard, GrF neat, GrF aged. Filling factors were kept as close to identical as possible, using a ruler to check the final heights after loading. The amount of sample powders loaded in P125E were **(i)** 23.4 mg for the Cu standard (equals to 5.95 mg of Cu^{2+}), **(ii)** 17 mg for neat GrF, and **(iii)** 12.6 mg for the aged GrF.

Evaluation of spin density (*Ds*) in GrF at the beginning and at the end of the aging process in DMF

Standard (ST): $CuSO_4 \times 5H_2O$, MW = 249.69

$N_A = 6.02214 \times 10^{23}$

N_A (ST) = 2.41×10^{21} (per molecule), or 9.48×10^{21} (per Cu^{2+} cation)

$$D_s\,(\mathrm{FG}) = \left(\alpha \times \frac{\iint \text{Signal Intensity FG}}{\iint \text{Signal Intensity Cu}_{ST}} \right) \times \frac{g_{ST}}{g_{FG}} \times N_{A,ST}$$

g_{ST} = grams of standard, g_{FG} = grams of GrF

α = g_{avg} values ratio, g_{ST}/g_{FG} = 2.170 (Cu) /2.000 (GrF) = 1.085

RESULTS:

GrF neat (t=0), Ds = 23.2×10^{18} spin/g

GrF (t=10 days), Ds = 5.4×10^{18} spin/g

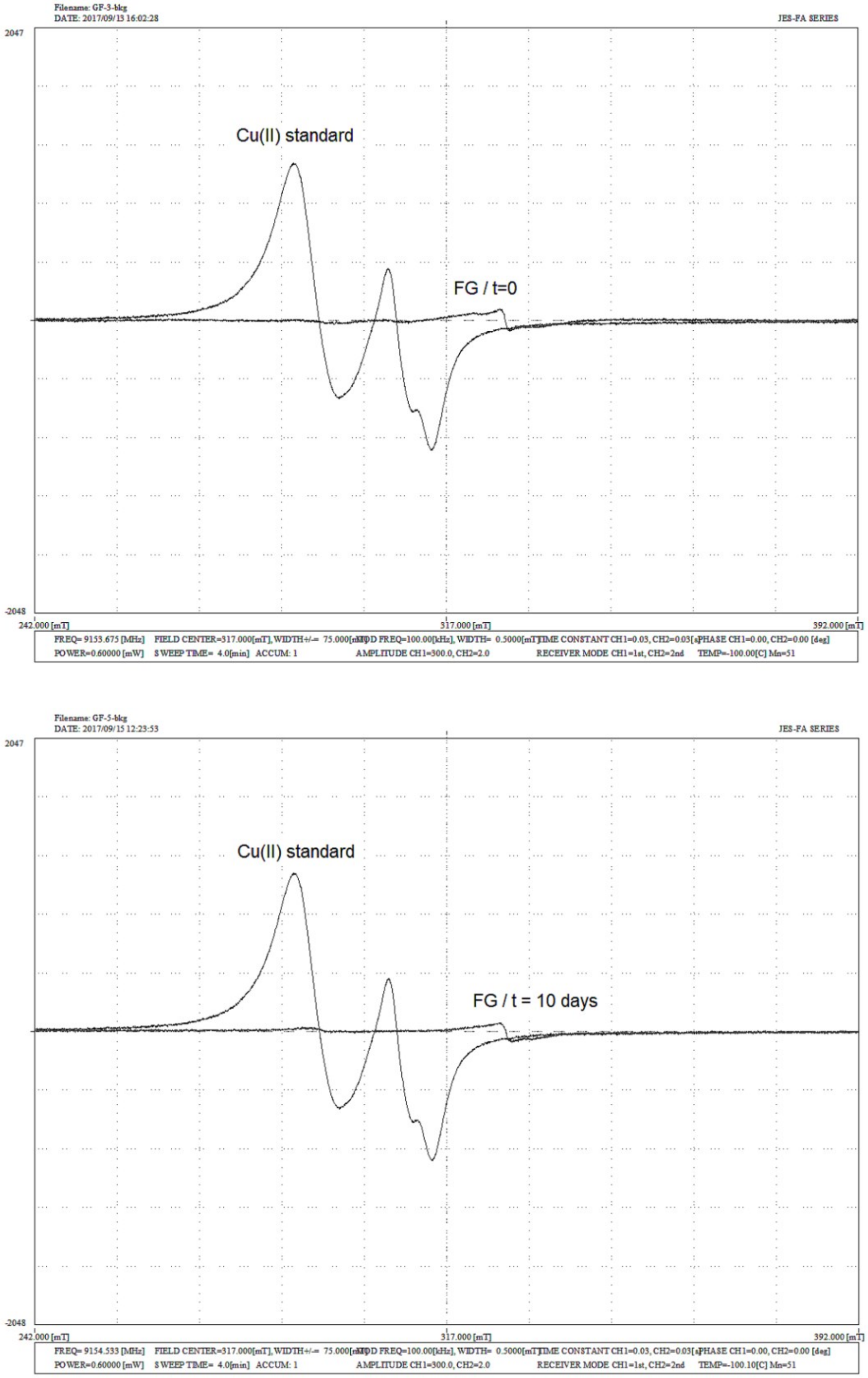

FREQ= 9153.675 [MHz] FIELD CENTER=317.000[mT], WIDTH+/-= 75.000[mT] MOD FREQ=100.00[kHz], WIDTH= 0.5000[mT] TIME CONSTANT CH1=0.03, CH2=0.03[s] PHASE CH1=0.00, CH2=0.00 [deg]
POWER=0.60000 [mW] SWEEP TIME= 4.0[min] ACCUM: 1 AMPLITUDE CH1=300.0, CH2=2.0 RECEIVER MODE CH1=1st, CH2=2nd TEMP=-100.00[C] Mn=51

FREQ= 9154.533 [MHz] FIELD CENTER=317.000[mT], WIDTH+/-= 75.000[mT] MOD FREQ=100.00[kHz], WIDTH= 0.5000[mT] TIME CONSTANT CH1=0.03, CH2=0.03[s] PHASE CH1=0.00, CH2=0.00 [deg]
POWER=0.60000 [mW] SWEEP TIME= 4.0[min] ACCUM: 1 AMPLITUDE CH1=300.0, CH2=2.0 RECEIVER MODE CH1=1st, CH2=2nd TEMP=-100.10[C] Mn=51

Figure S12 X-band EPR spectra (*T*= 173 K) of neat GrF (dried powder) at the beginning (t=0, upper spectrum) and after 10 days (lower spectrum) aging in DMF. The $CuSO_4$ powder spectrum, the spin standard used in the spin concentration analysis, has been plotted together with the GrF traces. The experimental parameters used within acquisition are reported in the plot legends.

1.3 Spin trap experiments on GrF/Benzene suspensions using POBN

The spin-trap molecule, α-4-pyridyl-1-oxide-N-*tert*-butylnitrone (POBN), was initially dissolved in benzene or in DMF (concentration of 11 mg/ mL), and the solutions aged at 40°C for 2 hours. These experiments were carried out to demonstrate that in these solvents there is no spontaneous degradation of the POBN precursor into a nitroxide spin-active species. Same negative results were obtained using sonication (in water bath, 1 hour) instead of mechanical stirring and mild heating. In the case of the GrF/benzene aging process, we demonstrated in the main manuscript text that no degradation of GrF (in terms of loss of the spin-active content) occurred in benzene. This observation has been further validated here, in presence of the POBN spin-trap agent. The experimental set-up used were as follows: addition of solid POBN (10 mg) to the GrF/benzene suspension (15 mg of GrF/1 mL of benzene) followed by incubation of the mixture for 40 min, centrifugation (10000 rpm) and collection of the supernatant, revealed that only a negligible amount of nitroxide radical species (just above the threshold of the background noise) can be detected by X-band EPR at low temperature. Figure S12a shows the negative result (X-band EPR spectrum) for the fluid solution (*T*= 253 K) and Figure S12b the correspondent extremely weak EPR spectrum detected in the frozen matrix (*T* = 123 K). Similar findings were obtained upon addition of solid POBN on other GrF/benzene suspensions previously aged either for 1 day or 6 days, following the same experimental procedures reported above. Thus, not only GrF in benzene remains stable, but it is clearly negligible the direct electron transfer between GrF to the POBN radical-trap.

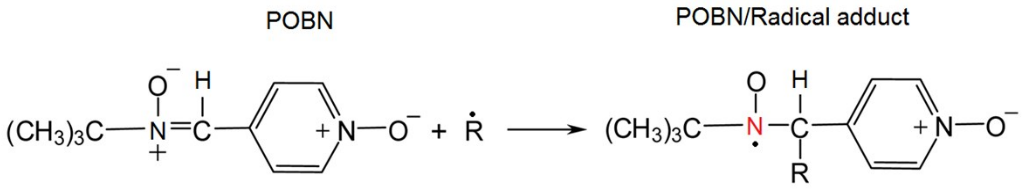

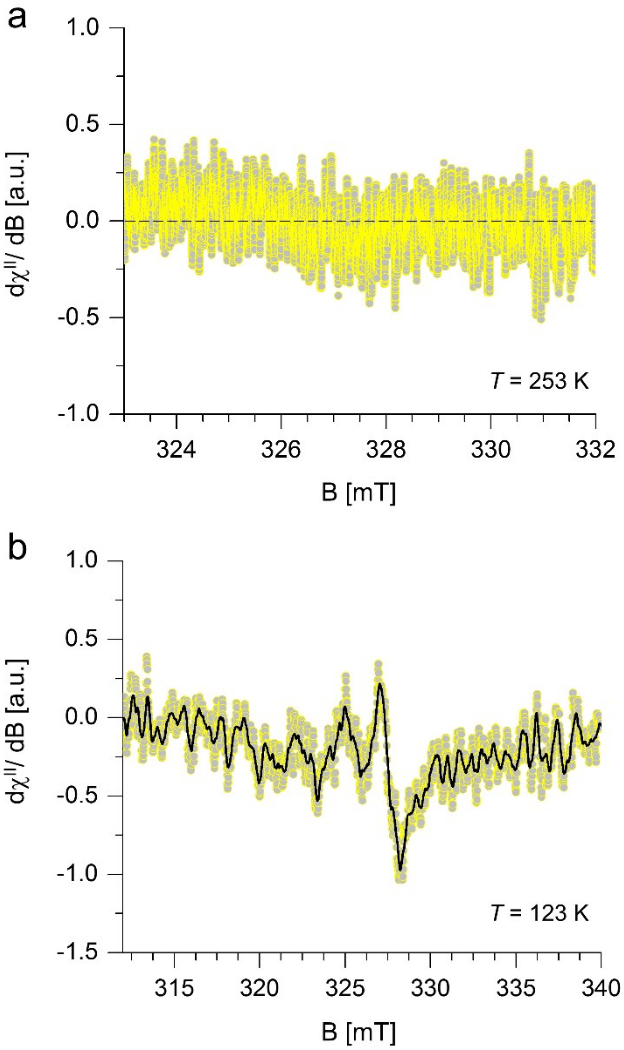

Figure S13 X-band EPR spectra of the spin-trap (POBN) experiments carried on the GrF/Benzene suspensions. (a) Solution spectrum (*T* = 253 K) of the supernatant from GrF/Benzene/POBN mixture and **(b)** its correspondent spectrum recorded in frozen matrix (*T* = 123 K). The solid black line in **(b)** corresponds to the resolution enhanced EPR resonance line (Savitzky-Golay, denoise algorithm). Experimental parameters: 9.16-9.17 GHz Frequency, 100 KHz modulation frequency, 30 ms time constant, 0.2 mT (**a,**) or 0.8 mT (**b,**) modulation width, 0.3 mW (**b,**) or 4.0 mW (**a,**) of applied microwave power

Spin trapping experiments carried out on GrF/DMF with POBN. The experimental set-up used were as reported for GrF/Benzene/POBN, namely: addition of solid POBN (10 mg) to the GrF/DMF suspension (15 mg of GrF/1 mL of DMF) followed by incubation of the mixture for 40 min, centrifugation (10000 rpm) and collection of the supernatant for EPR measurements. Below, in Figure S14, is shown the EPR spectrum of the whole mixture (frozen matrix) before collection of the supernatant.

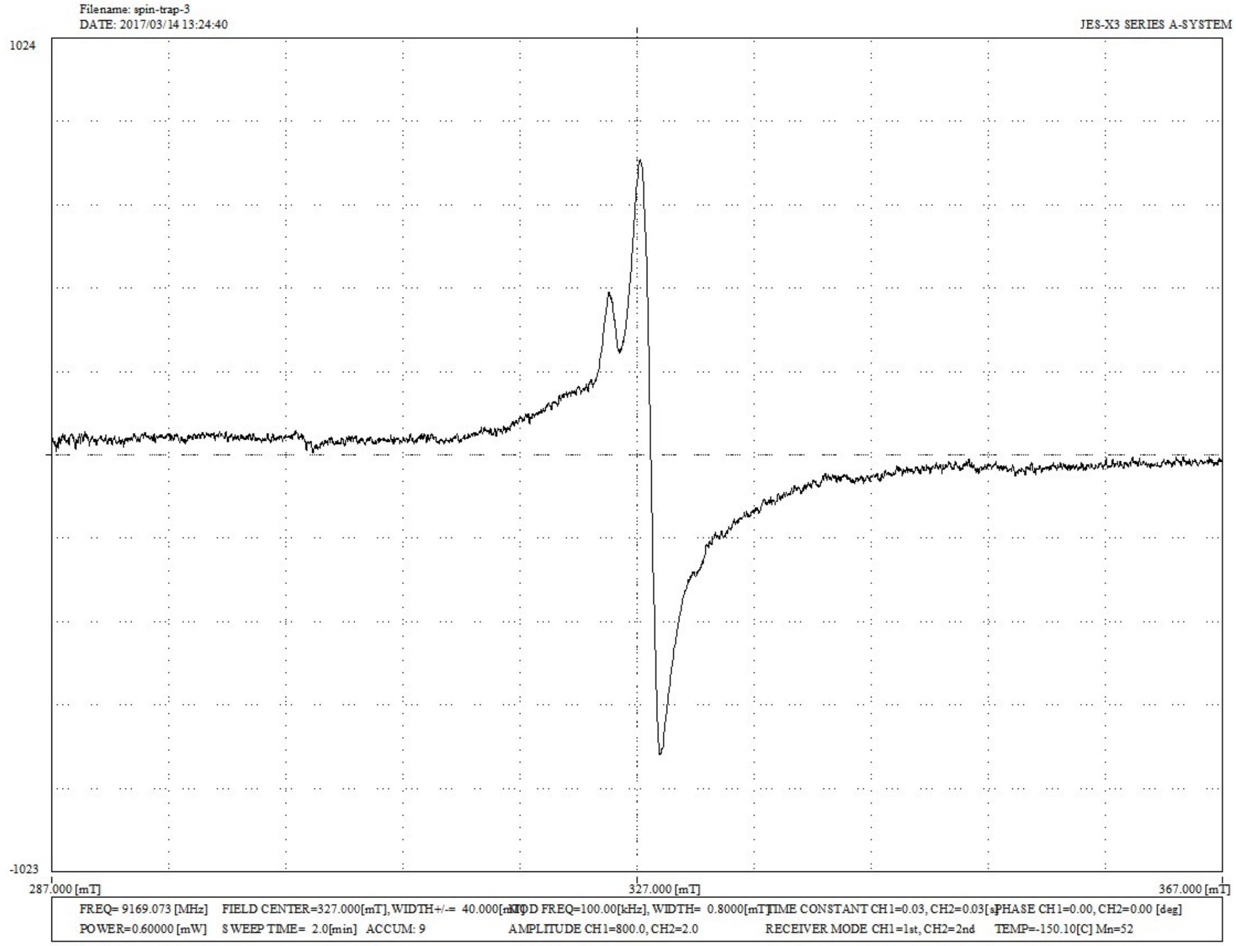

Figure S14 X-band EPR spectrum of the FG/DMF suspension in presence of the radical spin-trap POBN taken as the whole suspension (namely before collection of the supernatant only). Experimental parameters: 9.1690731 GHz frequency, 100 KHz modulation frequency, 30 ms time constant, 0.8 mT modulation-width, 0.6000 mW of applied microwave power, 2 min sweep-time, *T* of 123 K. 9 scans accumulated and averaged.

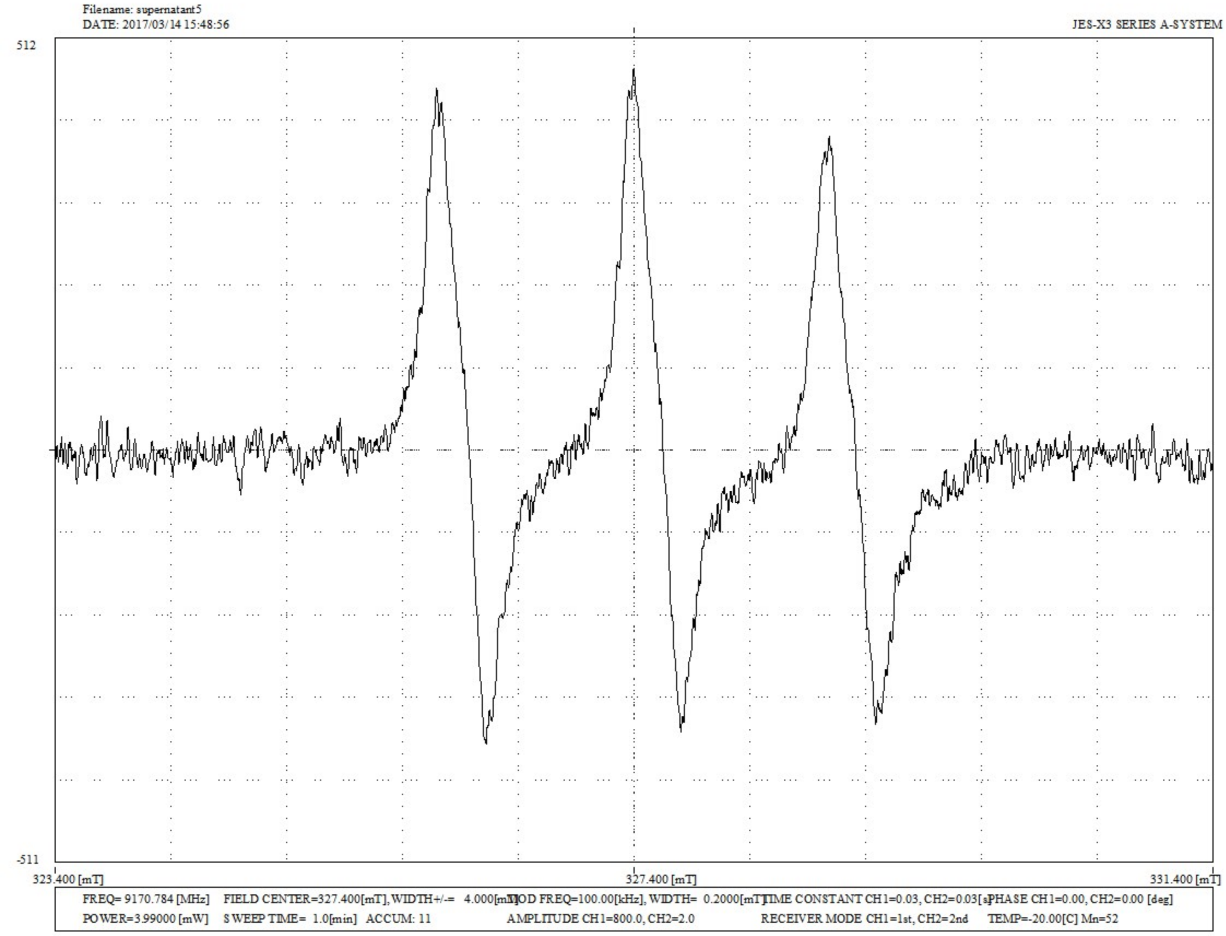

Figure S15 X-band EPR spectrum (T= 253 K) of the radical adduct collected in the supernatant from the reaction among GrF/DMF/POBN. The experimental parameters used within acquisition were as follows: 9.170784 GHz, 100.00 KHz mod. frequency, 0.2 mT modulation width, time const. 0.03 s, sweep time 1 min, microwave power 3.9900 mW, 11 scan, T = 253 K. The spectrum can be simulated (WinEPR SimFonia software) using the following spin-Hamiltonian parameters: g_{iso} = 2.0049, $1A_{\mathrm{N}}$ = 1.340 mT (37.55 MHz), $1A_{\mathrm{H}}$ = 0.172 mT (4.82 MHz), L_{w} = 0.210 mT (5.88 MHz), Lorentzian/Gaussian ratio = 0.20. The accuracy of g_{iso} was obtained by recording the radical signal together with Mn(II)MgO standard (JEOL internal reference standard, Mn(II), g_{eff} = 2.00101±0.00005) as shown in Figure S16.

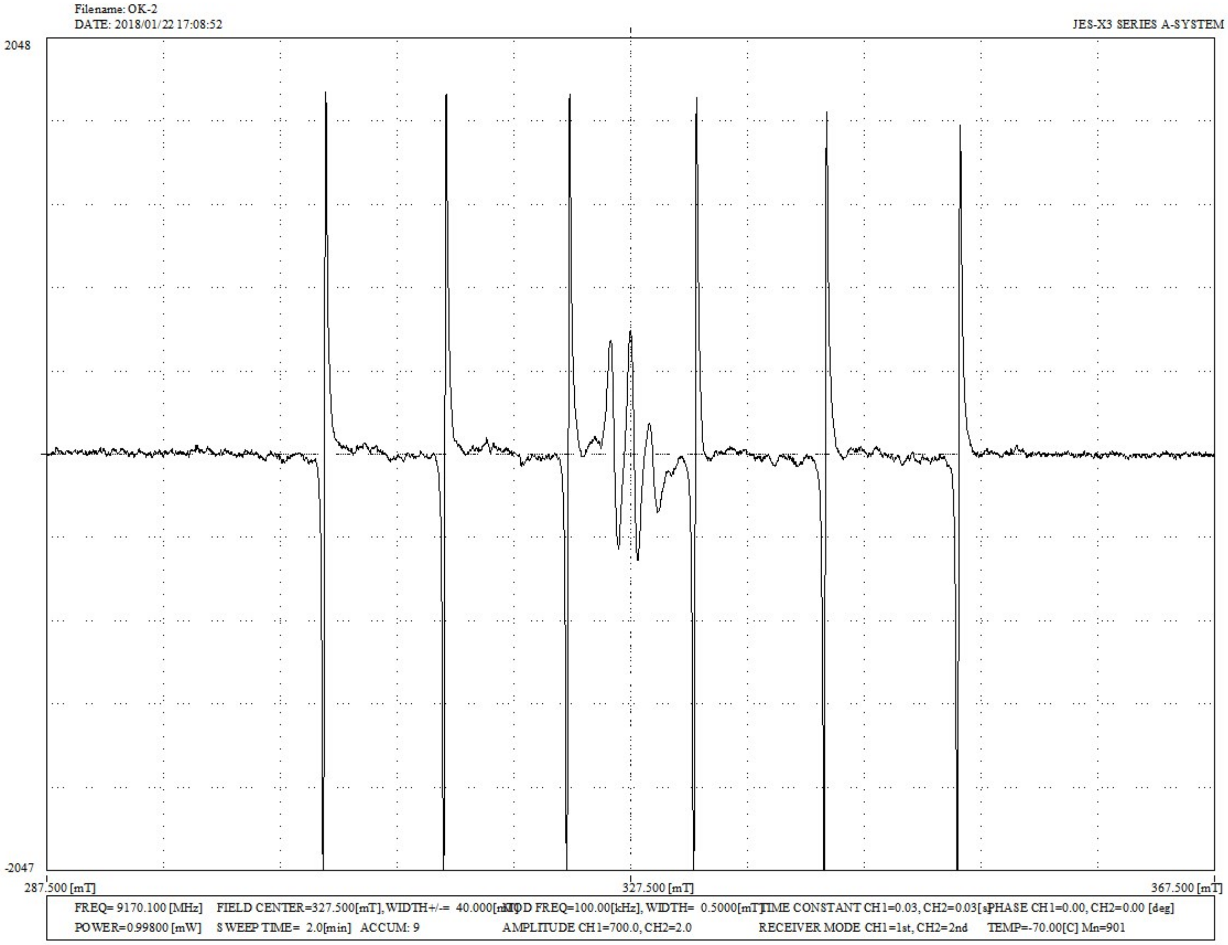

Figure S16. X-band EPR spectrum of GrF/DMF/POBN supernatant recorded together with Mn(II)MgO standard (JEOL internal reference standard, Mn(II), g_{eff} = 2.00101±0.00005). Experimental parameters: 9.170100 GHz, 100.00 KHz mod. frequency, 0.5 mT modulation width, time const. 0.03 s, sweep time 2 min, microwave power 0.9980 mW, 9 scan, T = 203 K.

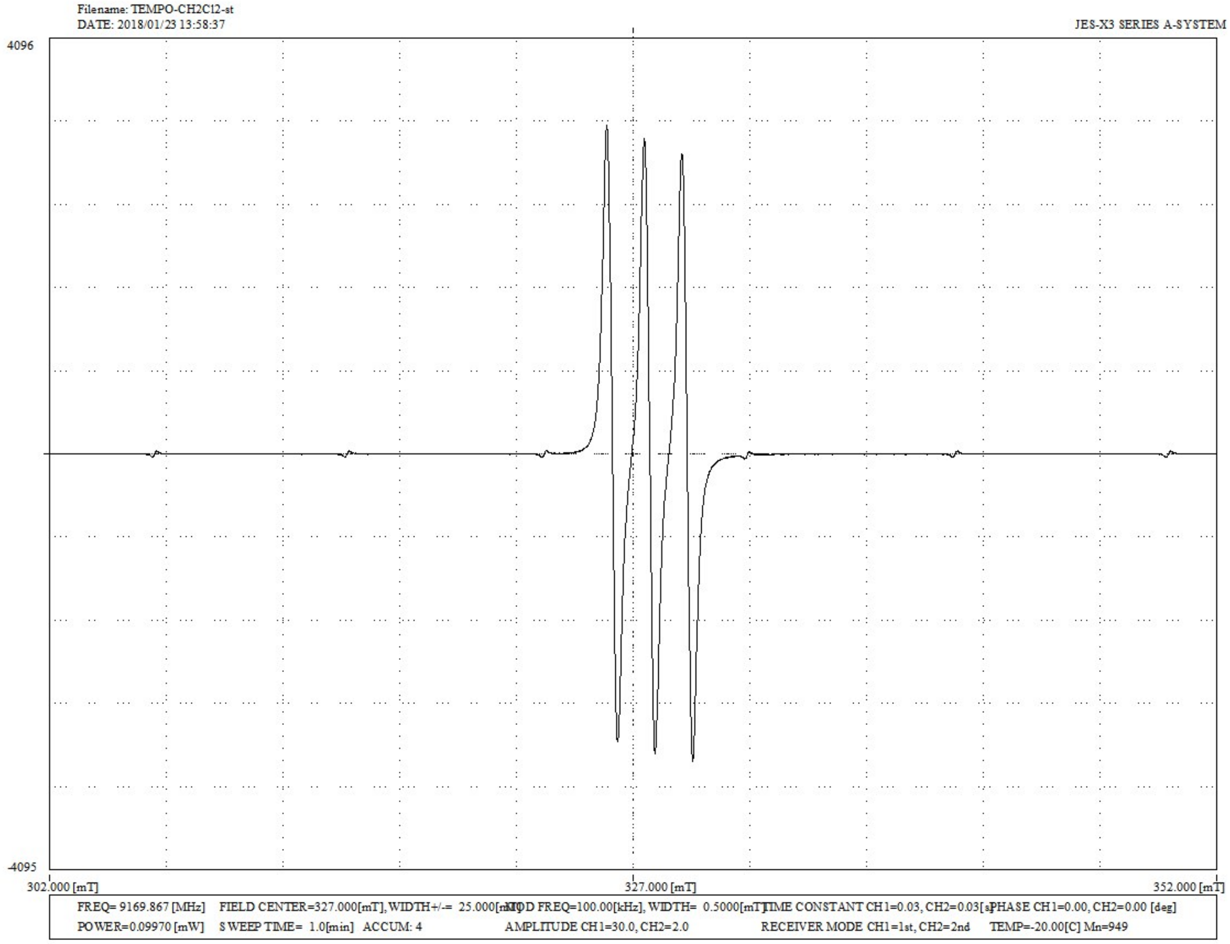

Figure S17. X-band EPR spectrum of the TEMPO radical (DMF/CH_2Cl_2 solution, 1/10, vol/vol) recorded together with Mn(II)MgO standard (JEOL internal reference standard, Mn(II), g_{eff} = 2.00101±0.00005) shown for comparison. Experimental parameters: 9.169867 GHz, 100.00 KHz mod. frequency, 0.5 mT modulation width, time const. 0.03 s, sweep time 1 min, microwave power 0.09970 mW, 4 scan, T = 253 K.

2,2,6,6-Tetramethyl-1-piperidinyloxy, free radical, 2,2,6,6-Tetramethylpiperidine 1-oxyl, TEMPO

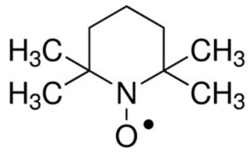

$g_{\mathrm{iso}} = 2.0057$, $A_{\mathrm{N}} = 1.54$ mT

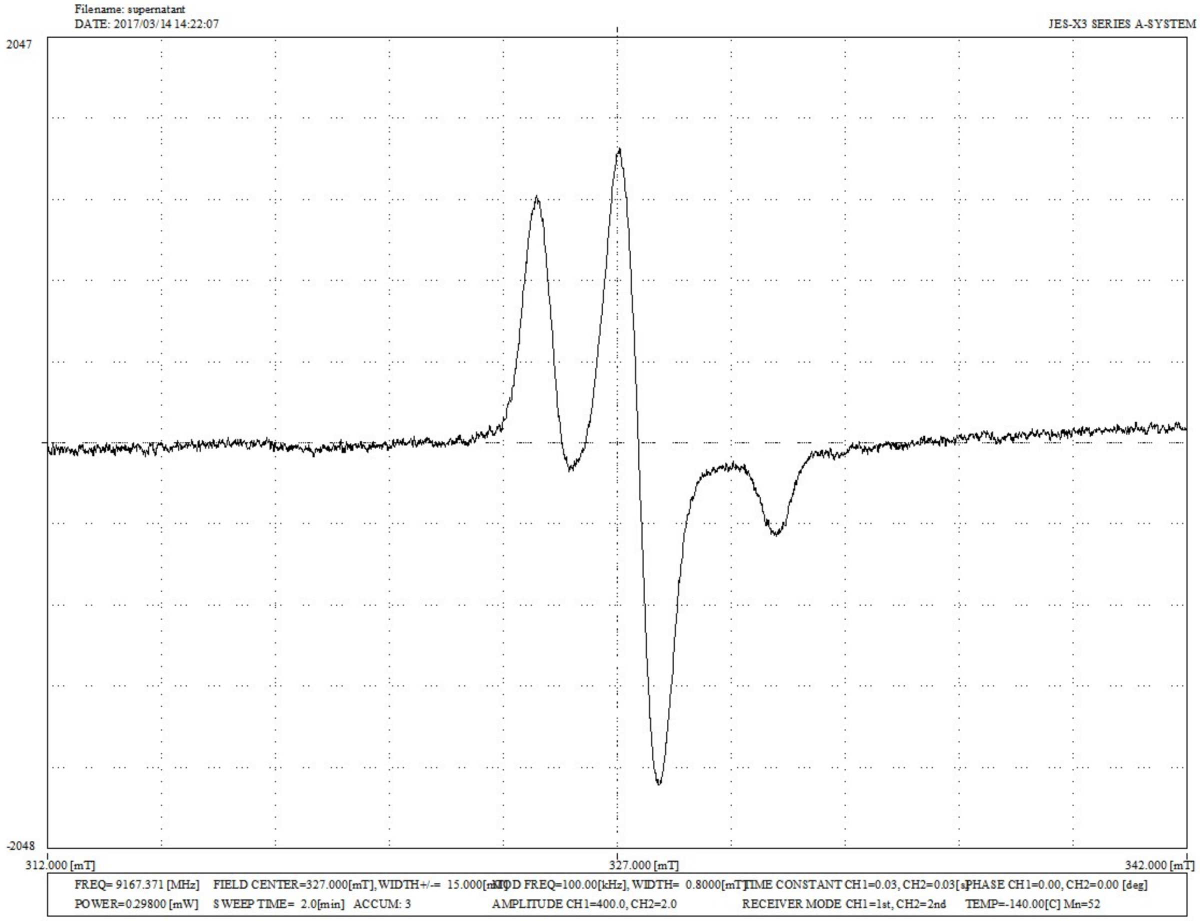

Figure S18 Frozen-matrix X-band EPR spectrum (*T*= 133 K) of the radical adduct collected in the supernatant from the reaction among GrF/DMF/POBN. The experimental parameters used within acquisition were as follows: 9.167371 GHz, 100.00 KHz mod. frequency, 0.8 mT modulation width, time const. 0.03 s, sweep time 2 min, microwave power 0.2980 mW, 3 scan. The spectrum can be simulated (WinEPR SimFonia software) using the following spin-Hamiltonian parameters: g_{xx} = 2.0066, g_{yy} = 2.0059, g_{zz} = 2.0022, $A(\mathrm{N})_{xx}$ = 0.40 mT, $A(\mathrm{N})_{yy}$ = 0.50 mT, $A(\mathrm{N})_{zz}$ = 3.15 mT, $L_{w(x,y,z)}$ = 0.70,1.10,0.80 mT, Lorentzian/Gaussian ratio =0.63 (number theta, phi of 200,200). The comparison of this radical signal with Mn(II)MgO standard (JEOL internal reference standard, Mn(II), g_{eff} = 2.00101±0.00005) is shown in Figure S19.

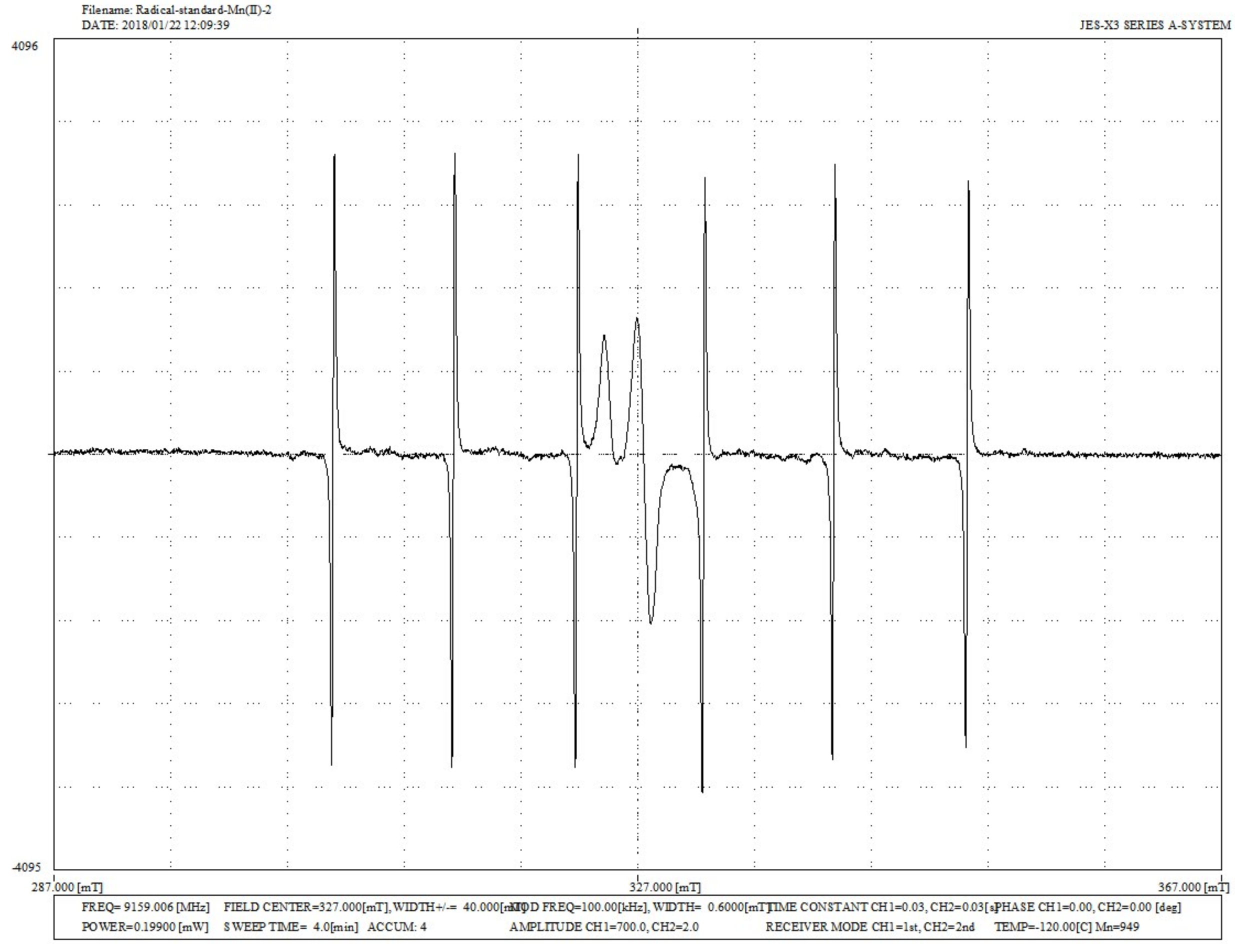

Figure S19 Frozen-matrix X-band EPR spectrum (*T*= 153 K) of the radical adduct collected in the supernatant from the reaction among GrF/DMF/POBN recorded together with Mn(II)MgO standard (JEOL internal reference standard, Mn(II), g_{eff} = 2.00101±0.00005). Experimental parameters: 9.159006 GHz, 100.00 kHz mod. frequency, 0.6 mT modulation width, time const. 0.03 s, sweep time 4 min, microwave power 0.19900 mW, 4 scan, *T* = 153 K.

Spin-trapping experiments under mild (water-bath) sonication (GrF/DMF/POBN).

Addition of solid POBN (10 mg) to the GrF/DMF suspension (15 mg of GrF/1 mL of DMF) followed by sonication (40 kHz) in water-bath for 30 min, then incubation of the mixture under simple mechanical stirring (400 rpm) for further 20 min at 40°C, centrifugation (10000 rpm) and collection of the supernatant for EPR measurements, lead to the appearance of an admixture of radical signatures. Figure S20, S23, shows the observed EPR spectra, which are clearly different from those obtained without sonication (see earlier EPR traces in Figure S18, S15 for comparison).

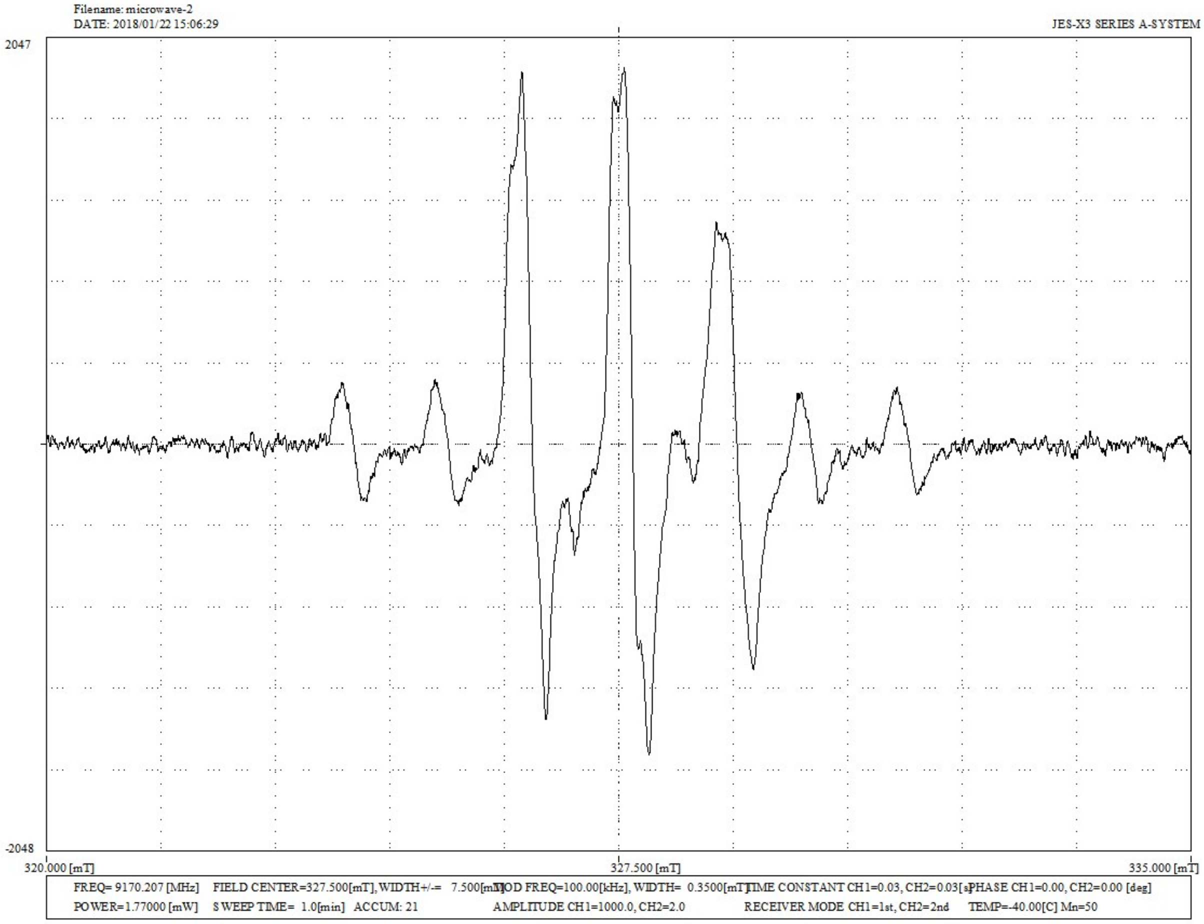

Figure S20. X-band EPR spectrum of GrF/DMF/POBN supernatant collected after mild sonication of the mixture. Experimental parameters: 9.170207 GHz, 100.00 kHz mod. frequency, 0.35 mT modulation width, time const. 0.03 s, sweep time 1 min, microwave power 1.7700 mW, 21 scan, $T = 233$ K.

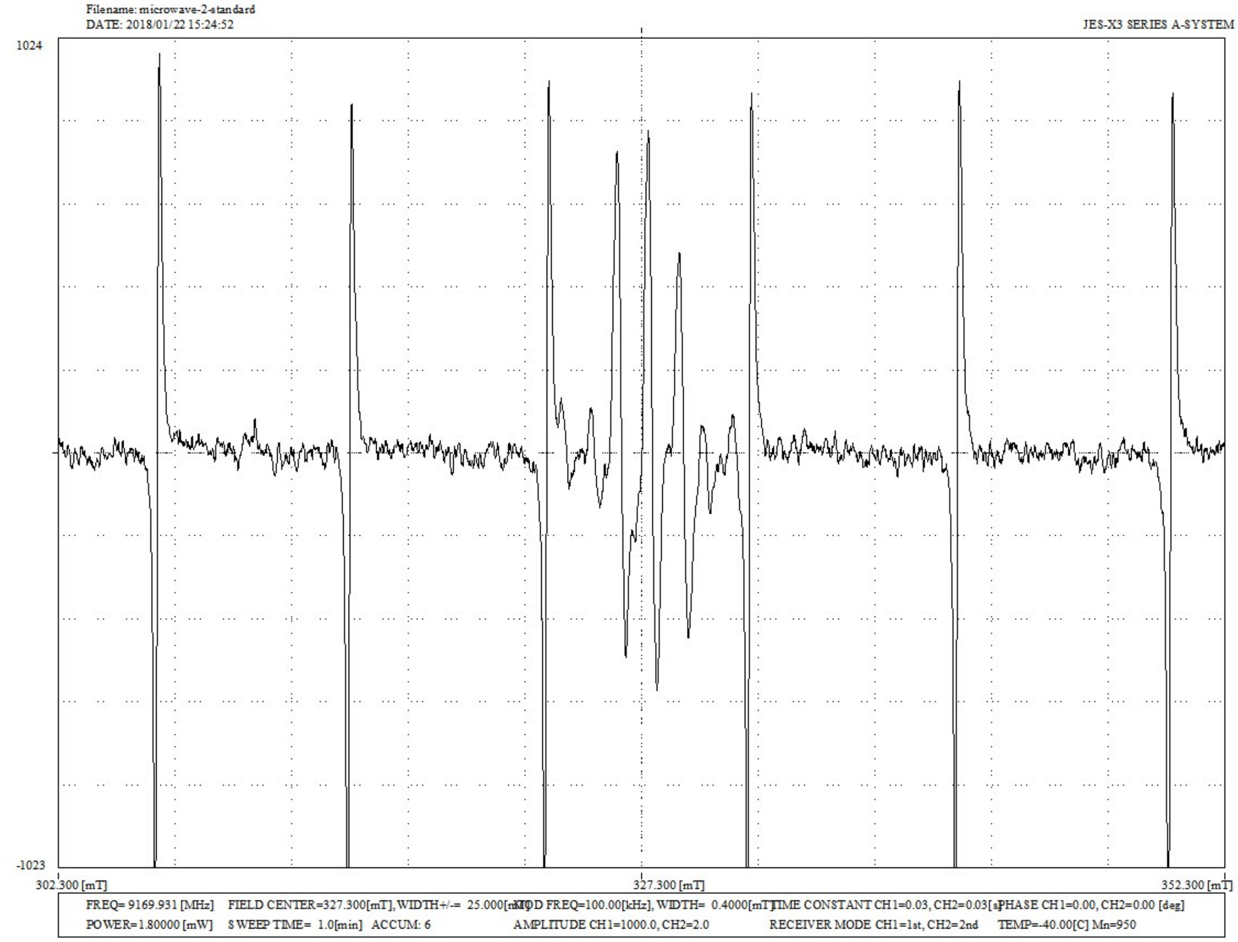

Figure S21 X-band EPR spectrum (*T*= 233 K) of the radical adduct collected in the supernatant from the reaction among GrF/DMF/POBN under mild sonication recorded together with Mn(II)MgO standard (JEOL internal reference standard, Mn(II), g_{eff} = 2.00101±0.00005). Experimental parameters: 9.169931 GHz, 100.00 kHz mod. frequency, 0.4 mT modulation width, time const. 0.03 s, sweep time 1 min, microwave power 1.8000 mW, 6 scan.

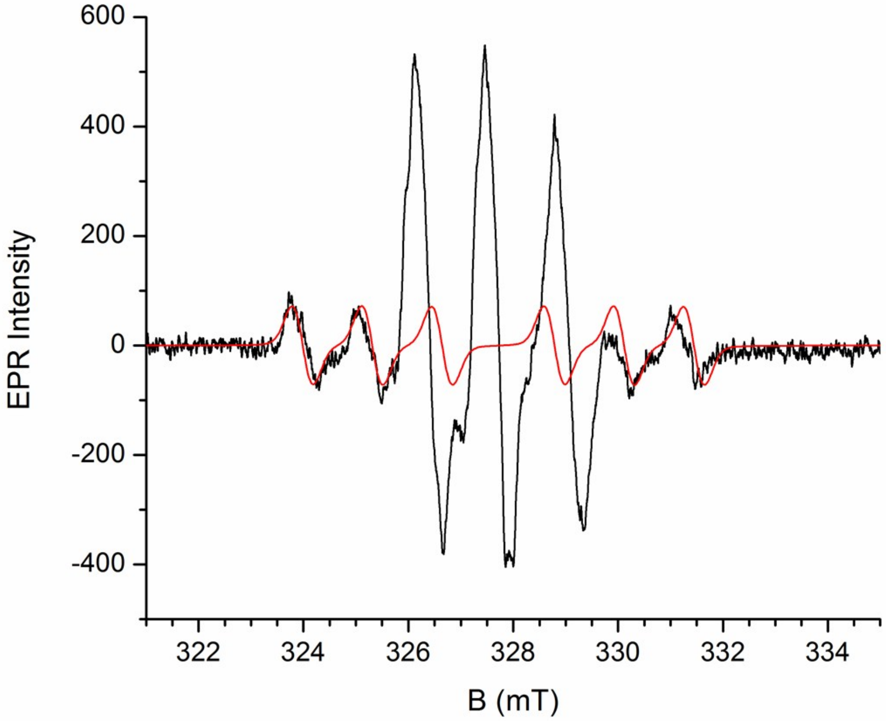

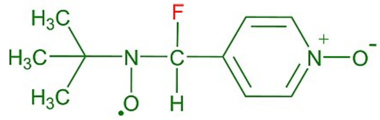

g-eff = 2.0046

1 A_N = 1.33 mT

1 A_H = 0.12 mT

1 A_F = 4.8 mT

L_w = 0.38 mT

L/G = 0.63

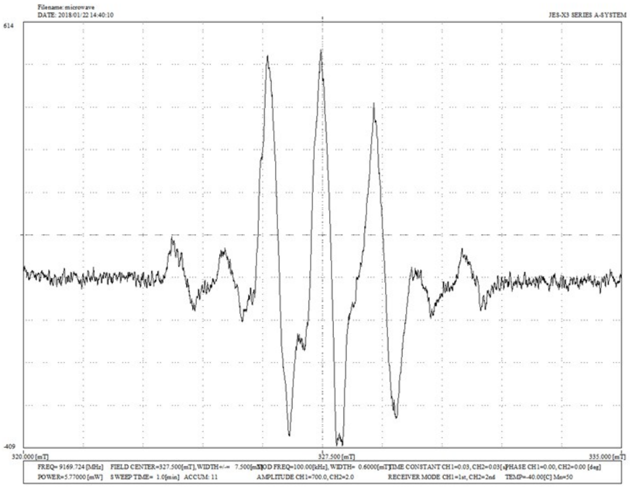

Filename: microwave
DATE: 2018/01/22 14:40:10
JES-X3 SERIES A-SYSTEM

FREQ= 9169.724 [MHz] FIELD CENTER=327.500[mT], WIDTH+/-= 7.500[mT] MOD FREQ=100.00[kHz], WIDTH= 0.6000[mT] TIME CONSTANT CH1=0.03, CH2=0.03[s] PHASE CH1=0.00, CH2=0.00 [deg]
POWER=5.77000 [mW] SWEEP TIME= 1.0[min] ACCUM: 11 AMPLITUDE CH1=700.0, CH2=2.0 RECEIVER MODE CH1=1st, CH2=2nd TEMP=-40.00[C] Mn=50

Figure S22. Tentative EPR simulation/parameters (red-line) assuming formation of a fraction of POBN-F radical adduct, as minor spin component entrapped during the GrF/DMF/POBN reaction performed under mild sonication (see notations on page S24). On the right, EPR spectrum recorded at 5.77 mW, 1 min sweep time, 0.6 modulation width, 233 K, 11 scan.

Note: PBN-F radical adduct: A_N = 12.2 G, A_H = 1.18 G, A_F = 45.6 G, Solvent: Benzene.

Reference: G. R. Buettner. Spin Trapping: ESR parameters of Spin Adducts. Free Radical Biology and Medicine, 1987, Vol. 3, pp. 259-303.

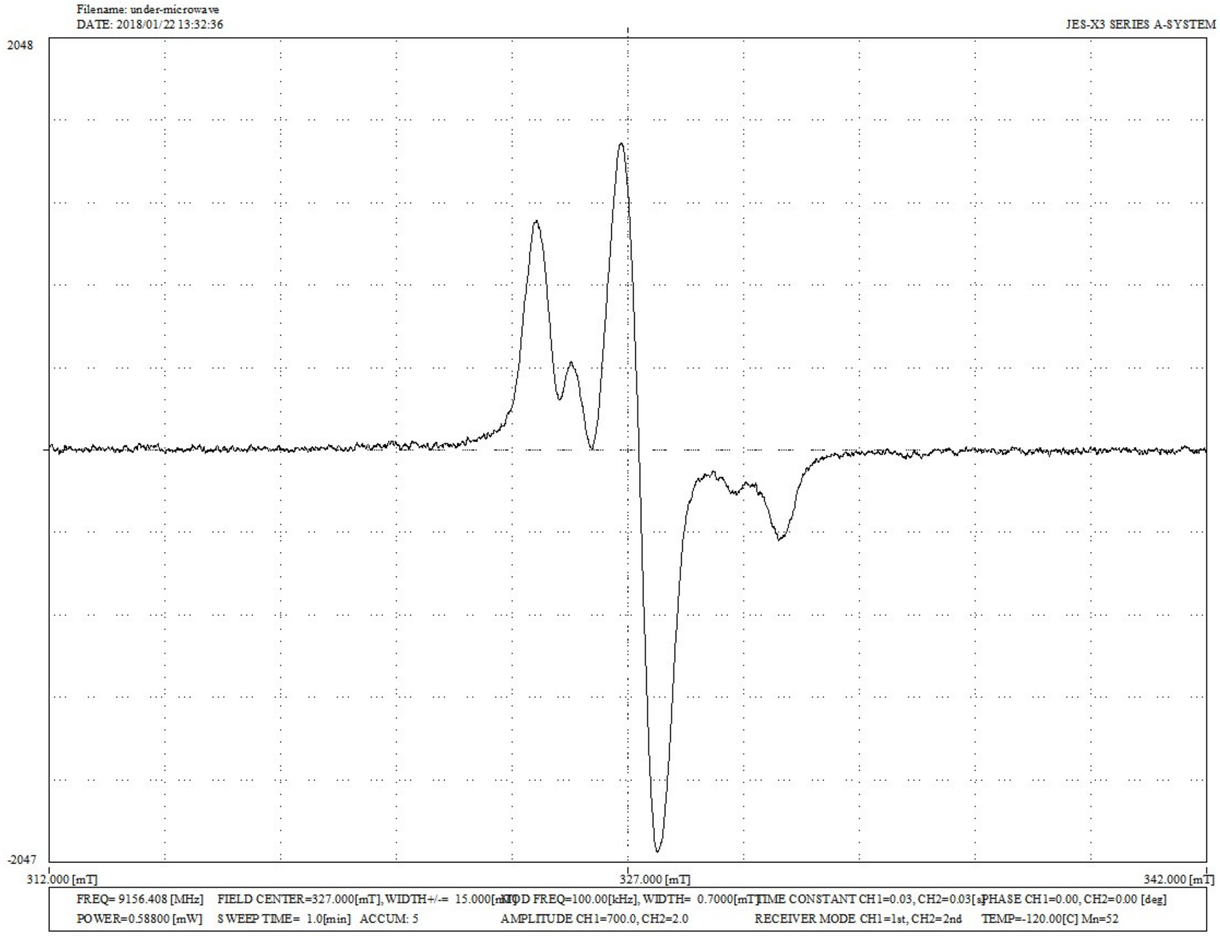

Figure S23 Frozen-matrix X-band EPR spectrum (*T*= 153 K) of the radical adduct collected in the supernatant from the reaction among GrF/DMF/POBN under mild sonication conditions. The experimental parameters used within acquisition were as follows: 9.156408 GHz, 100.00 KHz mod. frequency, 0.7 mT modulation width, time const. 0.03 s, sweep time 1 min, microwave power 0.5880 mW, 5 scan.

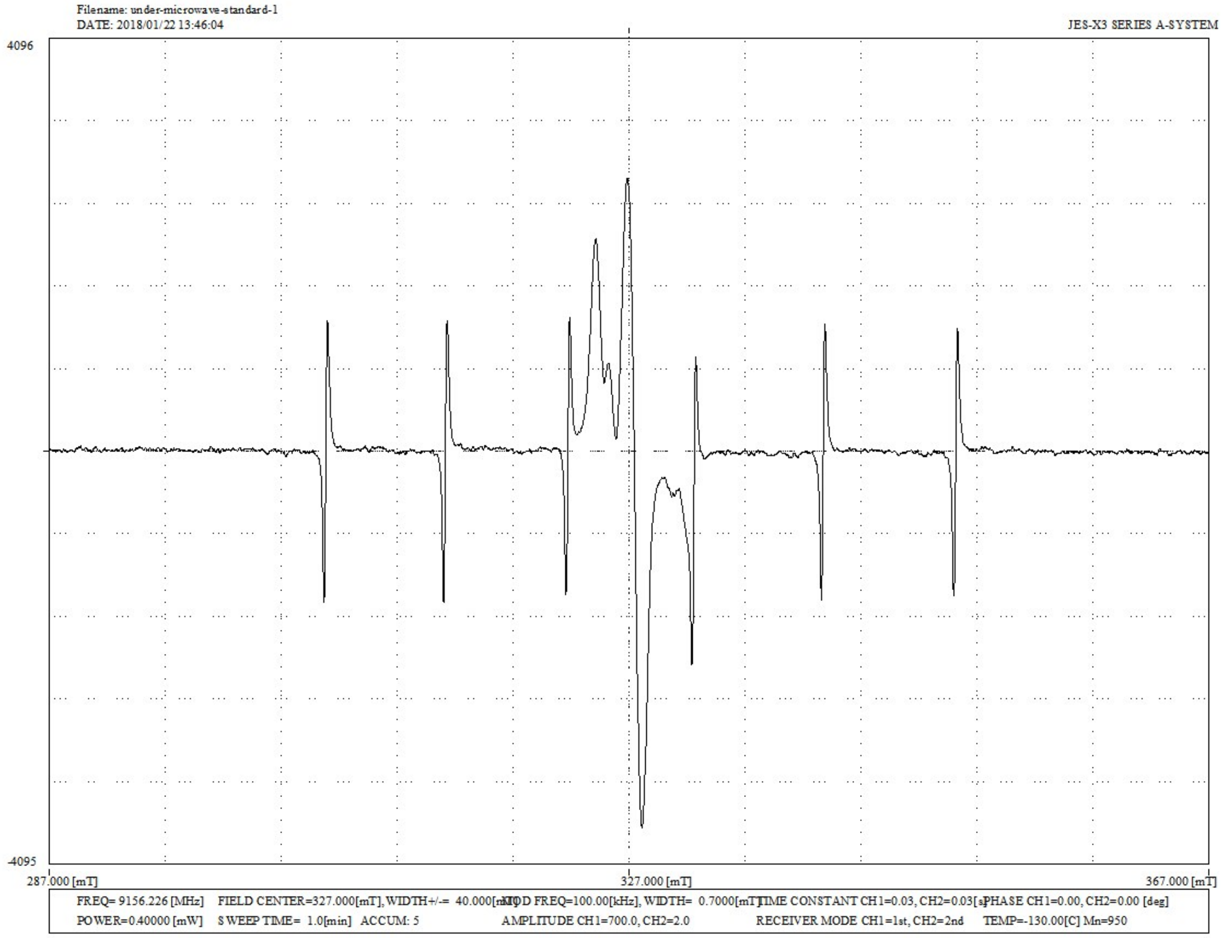

Filename: under-microwave-standard-1
DATE: 2018/01/22 13:46:04

FREQ= 9156.226 [MHz] FIELD CENTER=327.000[mT], WIDTH+/-= 40.000[mT] MOD FREQ=100.00[kHz], WIDTH= 0.7000[mT] TIME CONSTANT CH1=0.03, CH2=0.03[s] PHASE CH1=0.00, CH2=0.00 [deg]
POWER=0.40000 [mW] SWEEP TIME= 1.0[min] ACCUM: 5 AMPLITUDE CH1=700.0, CH2=2.0 RECEIVER MODE CH1=1st, CH2=2nd TEMP=-130.00[C] Mn=950

Figure S24 Frozen-matrix X-band EPR spectrum (*T*= 143 K) of the radical adduct collected in the supernatant from the reaction among GrF/DMF/POBN under mild sonication conditions recorded together with Mn(II)MgO standard (JEOL internal reference standard, Mn(II), g_{eff} = 2.00101±0.00005). The experimental parameters used within acquisition were as follows: 9.156226 GHz, 100.00 KHz mod. frequency, 0.7 mT modulation width, time const. 0.03 s, sweep time 1 min, microwave power 0.4000 mW, 5 scan.

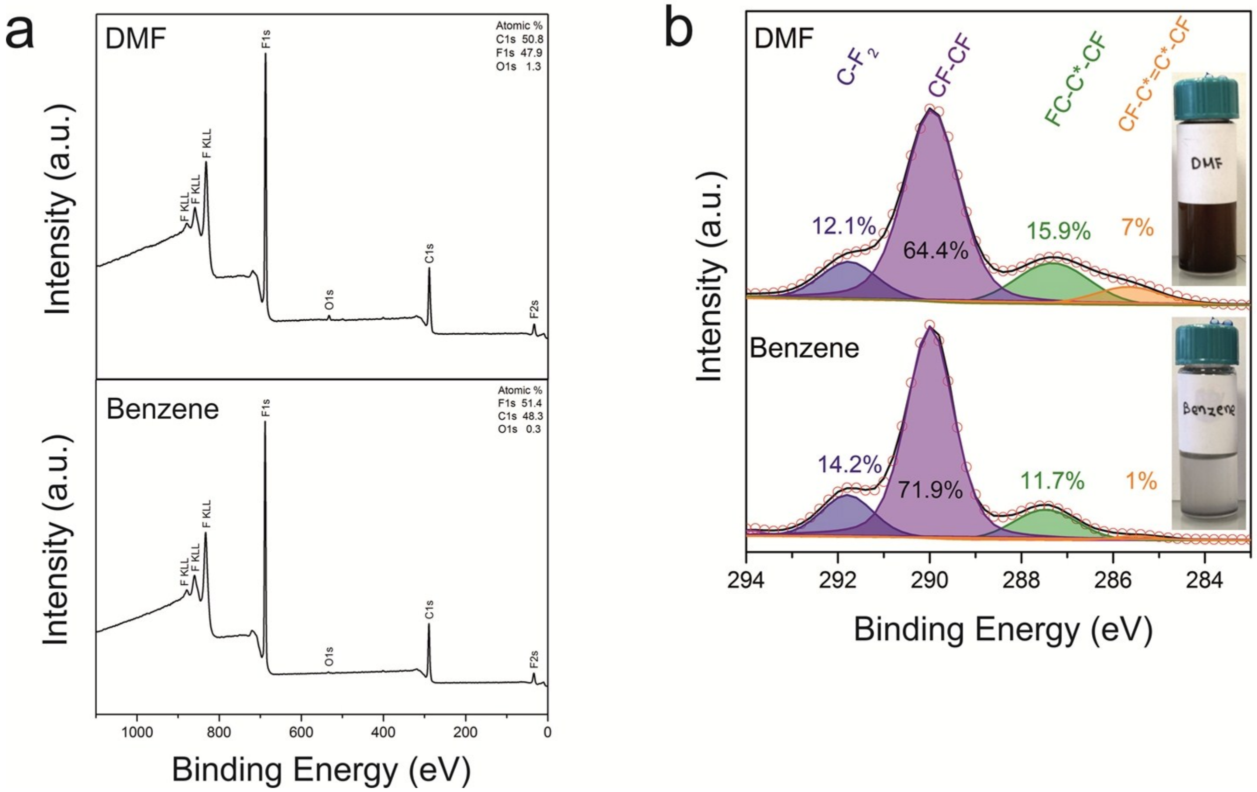

Figure S25 **(a)** Survey XPS spectra of GrF after 10-days-long aging in DMF (upper) and in benzene (lower), upon stirring at 40 °C under nitrogen (without any sonication), with C,F,O elemental percentages given in atomic %. The derived percentages clearly show that GrF is stable in benzene, where the composition of the material corresponds to the stoichiometry $C_{1.00}F_{1.06}$, i.e. practically the same as the starting composition given by the supplier of GrF ($C_{1.0}F_{1.1}$). In the case of the sample aged in DMF, the composition changed to $C_{1.00}F_{0.94}$ corresponding to ca 15 % of defluorination. **(b)** C 1s core level HR-XPS spectra. Deconvolution clearly confirms that the defluorination took place in the case of the DMF-treated sample (upper spectrum). This is indicated by the higher spectral areas corresponding to defluorinated carbons (FC-C*-CF and FC-C*=C*-CF components)[i] in comparison to the benzene-treated sample (lower spectrum). The inset photos provide direct visual evidence regarding the dramatic differences of the effect of the two solvents on GrF (photos taken after simple shaking for 6 h and without sonication). In benzene the color of GrF remains grey (as the pristine GrF), while in DMF GrF turns dark brown, due to the defluorination discussed in the main text.

1.4 F-DMF characterization

All samples used for the assessment of F-DMF formation were FG suspensions in DMF. FG was obtained from exfoliation of commercial graphite fluoride[ii] (starting concentration 5 mg/mL, 4h sonication with a Bandelin Sonorex, DT 255H type, frequency 35 kHz, power 640 W, effective power 160 W). The first sample was sonicated at T≤30 ºC for 2 hours and then stirred at room temperature overnight. The day after, the suspension was centrifuged (20000 rpm, 5 minutes) in order to isolate and analyze the supernatant liquid. No signal was visible in the ^{19}F NMR spectrum. The second sample was stirred at 120 ºC for 5 hours in a 10 mL round bottomed flask with reflux condenser under air, and at room temperature overnight. The day after, the black suspension was centrifuged (20000 rpm, 5 minutes) and the supernatant liquid was analyzed by ^{19}F NMR spectroscopy, revealing peaks at -26, -138 and -152 ppm (see Figure 7a, main text). Furthermore, F-DMF was prepared by fluorination of *N,N*-dimethylcarbamoyl chloride (Sigma-Aldrich) with KF/CaF_2 (Sigma-Aldrich, 1/4 weight ratio) in acetonitrile (Penta), following a literature procedure.[iii] Figure 7b (main text) shows the ^{19}F NMR spectrum of F-DMF in DMF. Then 5 µl of F-DMF were added to a suspension of FG in 1 mL DMF (FG concentration 5 mg/mL), heated at 120 ºC for 5 hours in a 10 mL round bottomed flask with reflux condenser under air and finally stirred at room temperature overnight. The day after, the black suspension underwent centrifugation (20000 rpm, 5 minutes) in order to separate the liquid for the insoluble parts. ^{19}F NMR analysis of the supernatant liquid revealed the peak of F-DMF at -26 ppm together with two small peaks at -138 and -152 ppm (see Figure S10).

NMR spectra were measured in DMF with JEOL ECA-500. ^{19}F NMR frequency 470MHz, shift calibrated on $CFCl_3$ (0 ppm). In each measurement, 0.5 mL of solution was used.

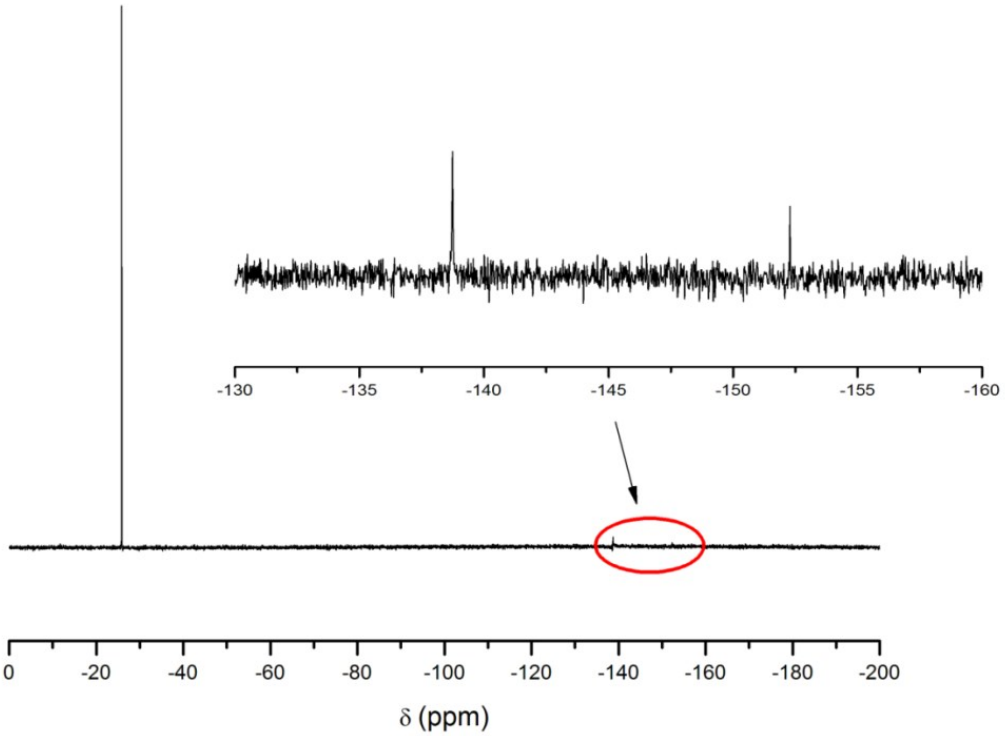

Figure S26 ^{19}F NMR spectrum (in DMF, 470 MHz) of) of the **clear** supernatant liquid obtained **after centrifugation (20000 rpm, 5 minutes) of** a GF/DMF suspension with 5 μL of F-DMF added to it, heated at 120 ºC for 5 hours and stirred at room temperature overnight. The insert shows the detailed spectrum of the range between -130 and -160 ppm.

2 Computational studies

2.1 Computational details

The ground state (GS) structures of all the investigated species were optimized by the ωB97X-D method[iv] using the Pople type double zeta basis sets.[v] If not stated otherwise, the 6-31++G(d,p) basis set was used. For the open-shell system, the spin unrestricted formalism has been applied. The solvent effects were included by using the universal continuum solvation model based on solute electron density (SMD).[vi]

While the structures of small and medium size systems (F, F^-, HF, DMF, …) were fully relaxed in geometry optimizations, to mimic the semilocal flexibility of FG sheets, the FG-like structures were obtained by constrained geometry optimizations keeping the edge carbon atoms frozen. All calculations were performed with the Gaussian09[vii] program.

2.2 The vertical and adiabatic electron affinities for a series of medium size model fluorinated polycyclic hydrocarbons

In order to get a more detailed picture about the role of the C—F σ* orbitals and the ability to accept an electron by fluorinated polycyclic hydrocarbons (F-PHC), we computed the gas phase vertical (VEA) and adiabatic (AEA) electron affinities and the HOMO-LUMO gap at the ωB97X-D/6-31++G(d,p) level of theory for a series of medium size model F-PHC including *trans*-decafluoronaphthalene (**1**), *trans*-tridecafluorophenalene (**2**), *trans*-tetracosafluorocoronene (**3**) (see Figure S27), and their radical counterparts), which corresponded to structures obtained from parent molecules by homolytic abstraction of a fluorine atom from the "central" tertiary carbon. We found (see Table S1) that for closed-shell systems the VEA values were negative and even AEAs taking into account the geometry relaxation of the corresponding radical anions were very small, which indicated rather low stability of the negatively charged species. We note that our DFT results were in very good agreement with those obtained with the MP2 method using the same basis set. Although the VEA values increased with increasing size of the F-PHC systems due to a possibility of larger delocalization of the negative charge, it can be expected that even for larger (perfect) FG structures the electron affinity would be very small. The evolution of the VEA values with the system size was in line with the qualitative picture provided by the HOMO/LUMO analysis. The positive LUMO energies and rather large HOMO-LUMO gap in closed-shell systems supported the idea about their low electron acceptor strength. In order to corroborate the involvement of the C—F σ* orbital, in Figure S27 we also show the shape of the LUMO for the three investigated F-PHC species. As anticipated by Sandford and others, the orbital has σ* character and it is mainly located on the central tertiary carbon atom. In line with our results on EA, the extent of its delocalization increases with the system size. To sum up, although the energetically low-lying C—F σ* orbital plays doubtlessly an important role in fluorine chemistry (e.g. through the orbital mixing as explained by Borden applying the second-order perturbation theory[viii] and even specifically in the defluorination reactions of PFCs when using suitable reducing agents under special catalytic conditions, it is improbable that mild reducing agents could initiate a radical cascade process of defluorination by a direct electron transfer to C—F σ* orbital on tertiary carbons in perfect C_1F_1 structures.

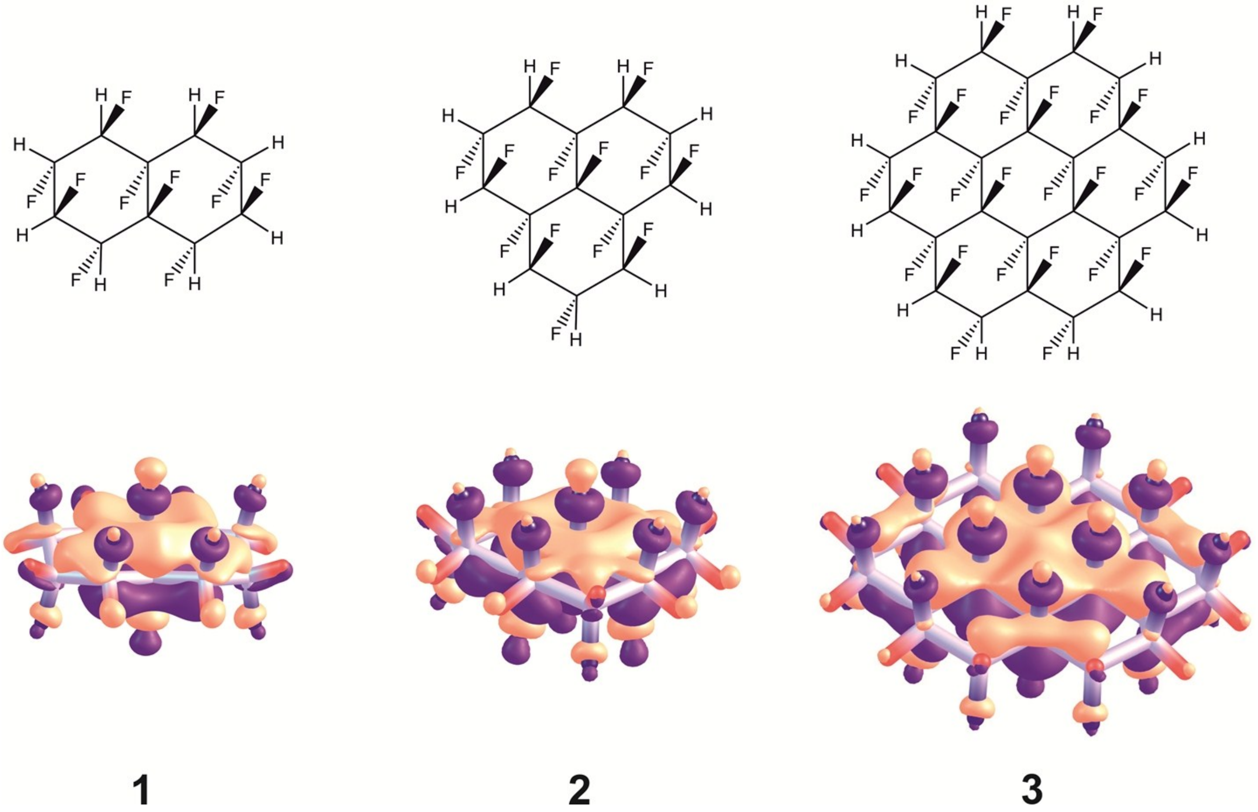

Figure S27 Formulas and the corresponding shape of the LUMO (C—F σ* orbital) for the three investigated F-PHC species.

Table S1 The gas phase vertical and adiabatic electron affinities (VEA and AEA) of fluorinated polycyclic hydrocarbons and corresponding radicals[a] **calculated at the ωB97X-D/6-31++G(d,p) level of theory.** The MP2/FC values are given in parentheses. HOMO/LUMO and the gap correspond to KS orbitals.

System	**VEA (kcal/mol)**	**AEA (kcal/mol)**	**HOMO (eV)**	**LUMO (eV)**	**HOMO-LUMO gap (eV)**
1	-21.0 (-20.7)	7.1	-11.08	0.97	12.05
2	-16.0 (-17.1)	12.0	-11.07	0.75	11.82
3	-3.3	4.0	-10.85	0.30	11.15
1 radical	53.5 (55.3)	67.2	-10.09	-2.15	7.94
2 radical	60.6 (63.0)	74.4	-10.34	-2.35	7.99
3 radical	66.8	80.6	-10.54	-2.46	8.07

[a] In the case of radical species, the LUMO/HOMO correspond to the lowest *β*(unocc)/highest *α*(occ) orbitals.

2.3 Other possible reactions in the FG/DMF system in the liquid phase

In Figure S28, we present processes that could potentially occur in the liquid phase above the FG surface. While the reactions (3a) and (3b) cannot be excluded at higher temperatures in polar solvents, the generation of F• radicals by reaction (3c) is improbable.

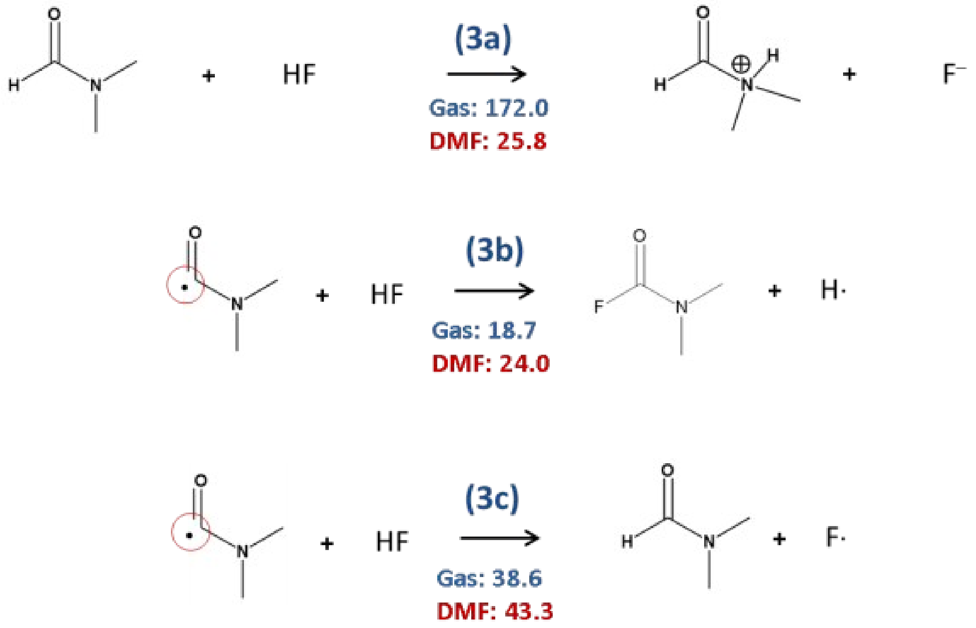

Figure S28 Other possible reactions in the liquid phase (above the FG surface) of the reaction mixture FG/DMF. The reaction energies are given in kcal/mol.

2.4 A radical mechanism of defluorination of FG in DMF starting from a biradical center

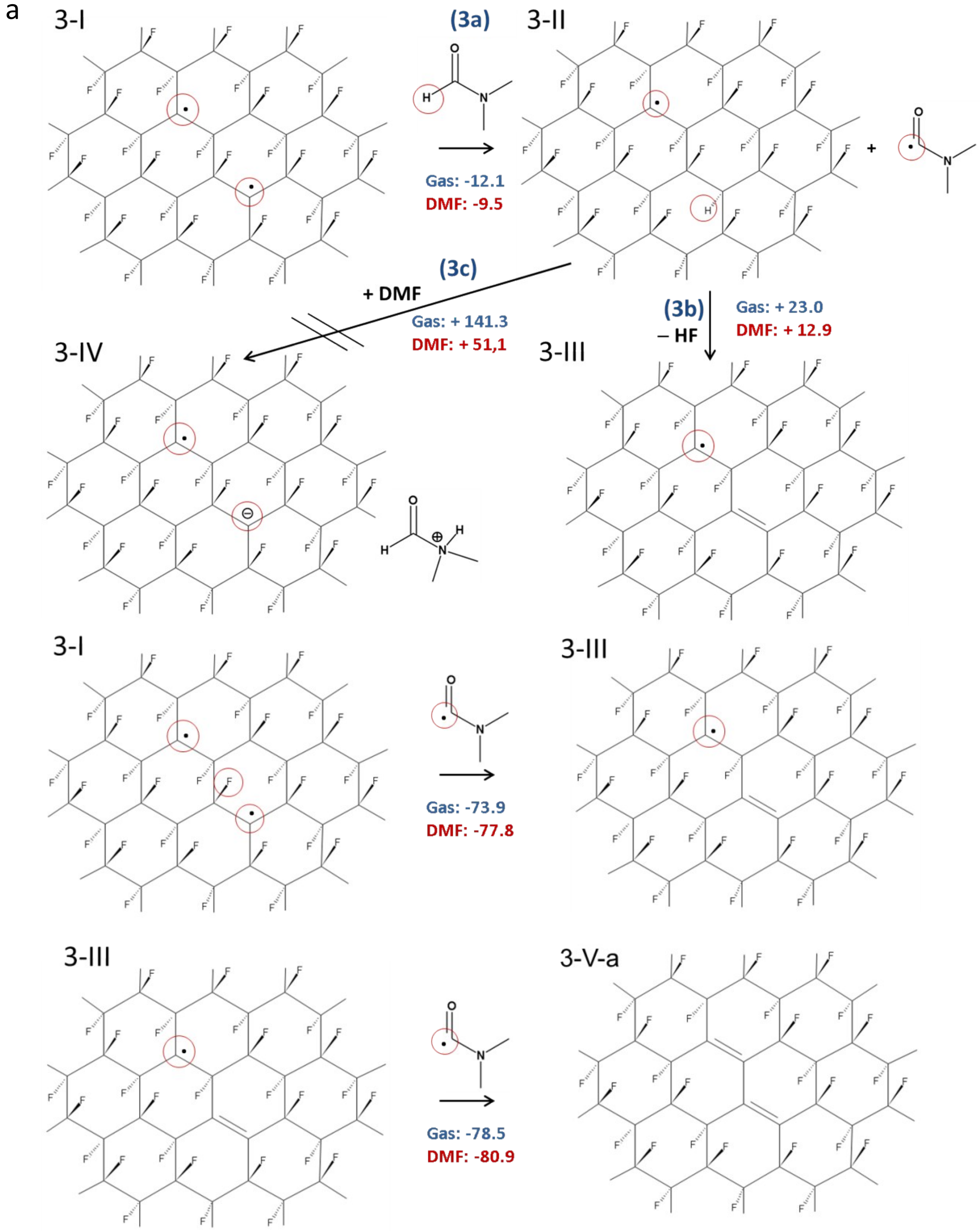

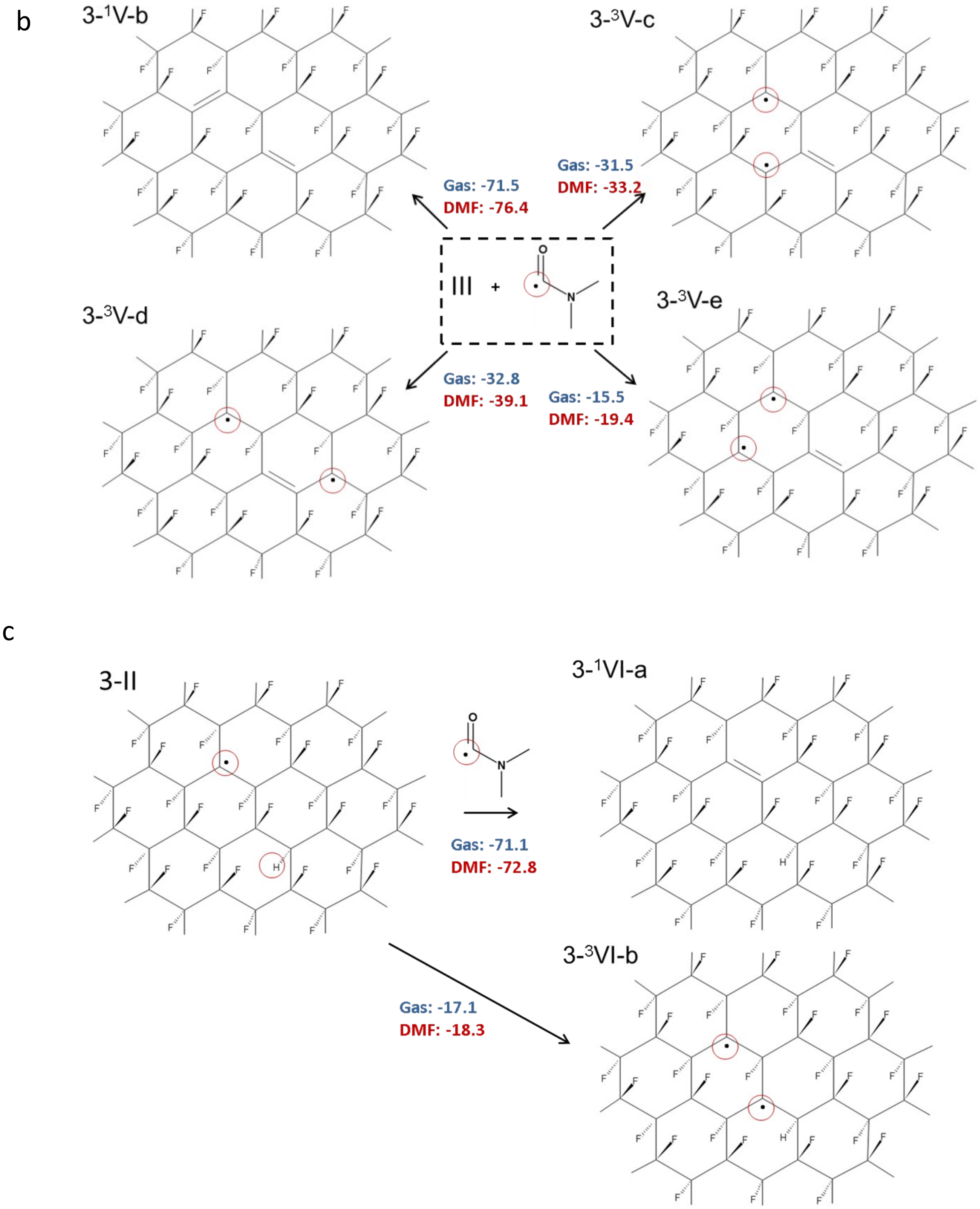
b
3-^{1}V-b
3-^{3}V-c
Gas: -71.5
DMF: -76.4
Gas: -31.5
DMF: -33.2
III +
O
N
3-^{3}V-d
3-^{3}V-e
Gas: -32.8
DMF: -39.1
Gas: -15.5
DMF: -19.4
c
3-II
3-^{1}VI-a
Gas: -71.1
DMF: -72.8
3-^{3}VI-b
Gas: -17.1
DMF: -18.3
F
H

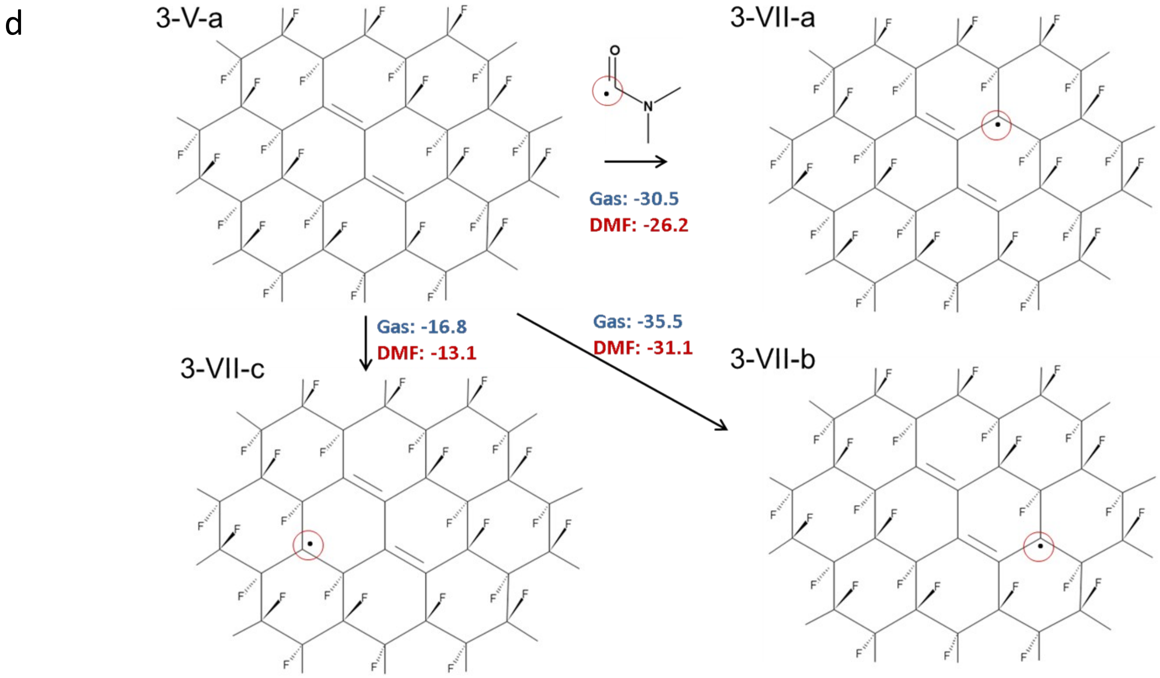

Figure S29 A radical mechanism of defluorination of FG in DMF starting from a biradical center. (a) Initial phases of defluorination. (b) Possible reactions of **3-III** with a DMF• radical. (c) Possible reactions of **3-II** with a DMF• radical. (d) Possible reactions of **3-Va** with a DMF• radical.

A note on possibility of a concerted proton coupled electron transfer (PCET) mechanism of the reaction (3a):

In PCET, the proton and the electron should start from different orbitals and should be transferred to different orbitals. Hypothetically such process could occur between a biradical FG structure and DMF but the similarity of energetics for monoradical and biradical cases (reactions (2a) in Figure 3 and (3a) in Figure S29) does not support this idea. Probability of the concerted mechanism would increase if two fluorine vacancies close to each other would exhibit a charge separation. This is however not the case, since the triplet state of **3-I** is more stable than any singlet state (the difference for the lowest singlet state is 47 kcal/mol at the ωB97X-D/6-31+G(d) level).

2.5 Validating the cluster models by extending their size and by PBC calculations

In order to validate the applicability of our finite size models in the analysis of FG reactivity we computed energy changes for the initial phases of reduction of FG for a larger model system at the same level of theory (see Figure S30). Our results confirm that the data presented in Figure 2 in the main text are reliable in the context of the system size.

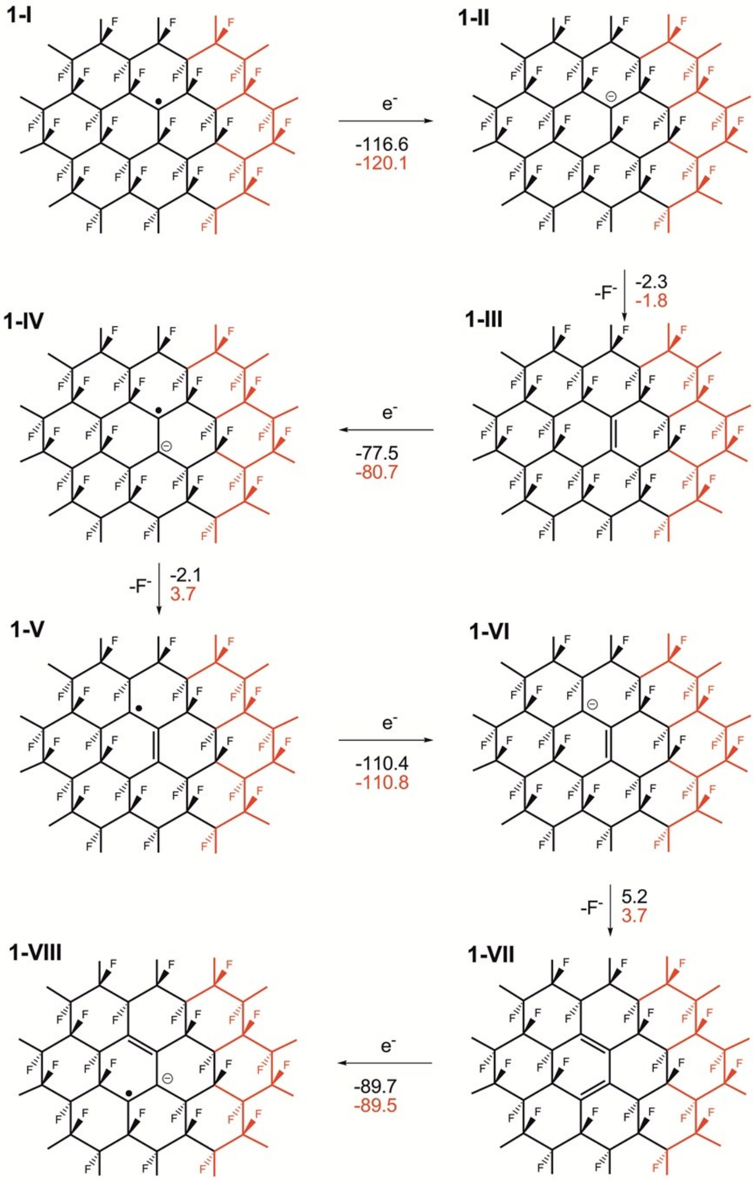

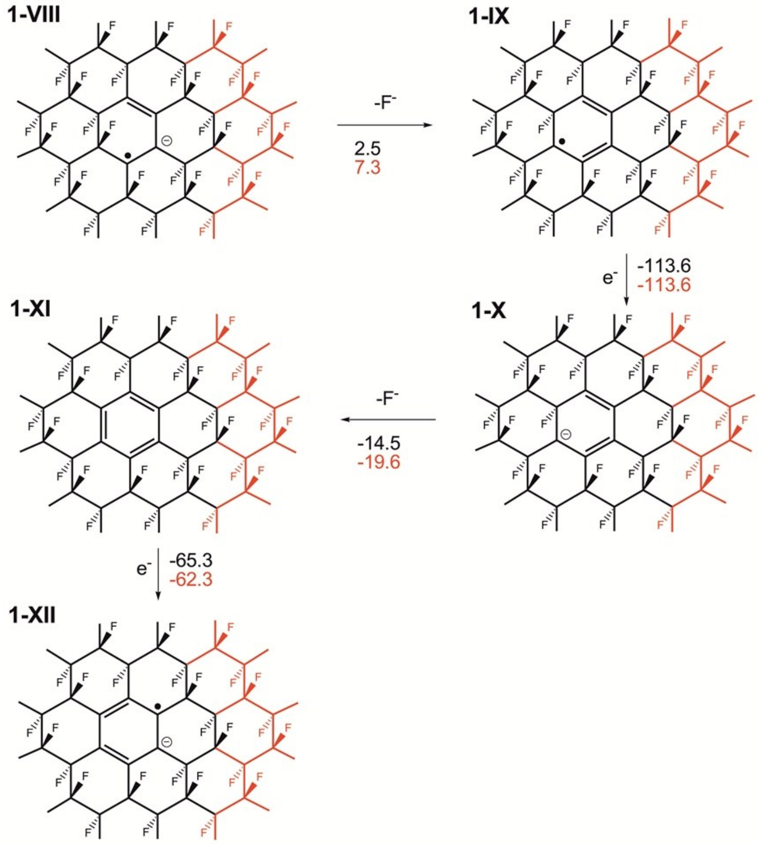

Figure S30 Scenario for the initial phases of reduction of FG. The reaction energies given in kcal/mol (black for black structures and red for the extended structures) were obtained at the *ω*B97X-D/6-31++G(d,p) level of theory.

To further support the validity of our finite-size model systems, we also performed plane-wave (PW) density-functional-theory (DFT) calculations with periodic boundary condition (PBC) for selected reactions (see Table S2) involving neutral species occurring in the reduction mechanism presented in Figure 2 (main text).

DFT-PBC computations were performed using the Vienna ab initio simulation package (VASP) [ix] employing the optimized van der Waals functional optB86b-vdW[x] for the exchange and correlation energy and projected augmented wave potentials (PAW) [xi-xii] to represent atomic cores. The wave functions were expanded in the PW basis set with a cutoff of 600 eV. Brillouin zone integrations were performed with a 3×3×1 Γ point-centered *k*-point mesh per 4×4 supercell (structure and cell optimization) containing 32 carbon atoms. A full structural optimization was performed using a quasi-Newton algorithm with a threshold of 0.02 eV $Å^{-1}$. The spin states of closed shell and radical species were S = 0 and S = ½, respectively. The solvent effects were taken into account by the implicit solvation model. [xiii]

The selection of reactions was based on the requirement of charge neutrality of the unit cell. It can be seen that any reaction in Figure 2 involves either attachment or release of a charged particle (electron or F^-). Since breaking the neutrality of a unit cell can lead to potential problems in the PBC calculations (apparent charges have to be added), the validity of finite-size models was tested only for neutral species (i.e. **1-I**, **1-III**, **1-V**, …) by calculating reaction energies for transformations like

1-I → **1-III** + ½ F_2

The half of the energy of F_2 molecule is the standard reference state for fluorine chemical potential in all PBC calculations. In this manner, only neutral species are involved, all three can safely be treated by finite-size as well as PBC approaches and, as a result, one can test their mutual consistency. Let us underline that the formation of F_2 molecules is in this cases only formal.

Table S2 A comparison of reaction energies (in kcal/mol) of selected chemical transformations of neutral FG species evaluated by the PW-DFT-PBC and *ω*B97X-D (finite size) models.

Reaction	**Gas phase**		**DMF solvent**	
	DFT-PBC	*ω*B97X-D (cluster model)	DFT-PBC	ωB97X-D (cluster model)
1-I → **1-III** + ½ F_2	25.1	30.1	24.7	30.4
1-III → **1-V** + ½ F_2	65.6	69.3	65.1	69.7
1-V → **1-VII** + ½ F_2	38.0	43.4	37.5	44.1
1-VII → **1-IX** + ½ F_2	59.5	62.0	58.7	62.1
3-I → **3-III** + ½ F_2	26.0	28.3	25.4	25.8
3-III → **3-V** + ½ F_2	18.1	23.7	17.8	22.7

2.6 Interaction of DMF with fluorinated coronene

In order to verify a hypothesis suggested by Wang *et al.*, [xiv] we have calculated the interaction energy of a DMF molecule with an ideal FG surface by using the implicit SMD model to account for the polar DMF environment. In Figure S31 we present the optimized structure of the DMF···*trans*-tetracosafluorocoronene (F-coronene) complex. The orientation of the DMF molecule indicates that the interaction is governed by dipole-dipole interactions as anticipated Wang *et al.*. Nevertheless, although the interaction energy was indeed found to be relatively high (5.2 and 4.0 kcal/mol in the gas phase and DMF, respectively) compared to ordinary weakly interacting systems, it is still far below the dissociation energy of a C—F bond (~100 kcal/mol for F-coronene). Let us note that we have also estimated the basis set superposition error (BSSE) of the interaction energy by gas phase calculations to be ca 0.7 kcal/mol.

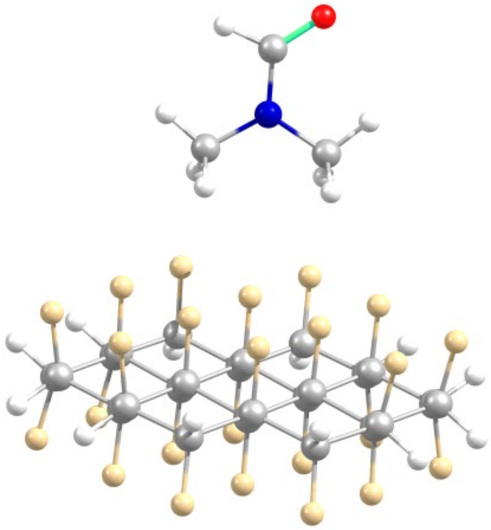

Figure S31 The optimized structure of the DMF···F-coronene complex

2.7 Isotropic Fermi Contact Couplings of POBN-F• and POBN-DMF• radicals

The qualitative differences in charge and spin density distribution together with isotropic Fermi contact couplings (FCC) *A* for the POBN-F• and POBN-DMF• radicals were analyzed at the B3LYP level using the tailored EPR-II and EPR-III basis sets as suggested by Barone.[xv] The data presented in Tables S3 and S4 and also Figures S32 and S33 show that in both cases the unpaired electron is mainly located on the nitrone moiety spreading towards the fluorine atom (in the case of POBN-F•), respectively towards the carbon atom of the trapped carbonyl radical (in the case of the POBN-DMF• radical). It can be seen that the EPR-II and EPR-III basis sets consistently describe the spin density distribution and related Fermi contact couplings. The Mulliken charges were found to be more dependent on the ability to describe the valence shell region by the used EPR basis sets. The solvent effects do not change the qualitative picture, nevertheless some *A* values (e.g. proton #17 couplings) are noticeably smaller for POBN-F in solution. Let us also note that the accuracy of theoretical values can also be affected by specific interactions that are neglected in implicit solvent models. In spite of these deficiencies, for nuclei with a spin quantum number $I > 0$ we achieved a reasonable agreement between theoretical (B3LYP/EPR-III/SMD) and experimental values, e.g., $A_{\mathrm{exp}}/A_{\mathrm{theor}} = 13.4$ G/11.2 G for N(#1) and $A_{\mathrm{exp}}/A_{\mathrm{theor}} = 1.7$ G/1.6 G for H(#17) in POBN-DMF.

Table S3 Isotropic Fermi Contact Couplings (in G), Mulliken charges, and atomic spin density on selected atoms for the **POBN-F** radical calculated with the B3LYP using the EPR-II and EPR-III basis sets. The numbering of atoms is shown in Figure S16.

Method	Basis set	No.	Type	A (G)	Charge	Spin density
POBN-F radical (gas phase)						
B3LYP	EPR-II	1	N(14)	9.65	0.14	0.39
		2	C(13)	-3.95	0.36	-0.01
		7	C(13)	4.12	-0.50	0.02
		15	O(17)	-13.93	-0.35	0.55
		16	C(13)	3.59	-0.10	0.02
		17	H(1)	0.99	0.14	0.00
		18	F(19)	51.55	-0.19	0.02
B3LYP	EPR-III	1	N(14)	9.47	-0.28	0.34
		2	C(13)	-3.96	0.89	0.00
		7	C(13)	4.06	-0.47	0.02
		15	O(17)	-15.34	-0.31	0.59
		16	C(13)	2.96	0.37	0.01
		17	H(1)	1.30	0.12	0.00
		18	F(19)	54.77	-0.24	0.02
POBN-F radical (DMF solvent, implicit solvation, SMD model)						
B3LYP	EPR-II	1	N(14)	9.34	0.17	0.42
		2	C(13)	-4.39	0.38	-0.02
		7	C(13)	4.80	-0.54	0.02
		15	O(17)	-13.76	-0.38	0.53
		16	C(13)	2.49	-0.07	0.02
		17	H(1)	0.10	0.19	0.00
		18	F(19)	56.64	-0.24	0.02
B3LYP	EPR-III	1	N(14)	9.19	-0.26	0.37
		2	C(13)	-4.41	1.02	-0.01
		7	C(13)	4.60	-0.52	0.02
		15	O(17)	-15.01	-0.38	0.56
		16	C(13)	1.47	0.47	0.01
		17	H(1)	0.16	0.18	0.00
		18	F(19)	57.95	-0.29	0.02

Table S4 Isotropic Fermi Contact Couplings (in G), Mulliken charges, and atomic spin density on selected atoms for the **POBN-DMF** radical calculated with the B3LYP using the EPR-II and EPR-III basis sets. The numbering of atoms is shown in Figure S17.

Method	Basis set	No.	Type	A (G)	Charge	Spin density
POBN-DMF radical (gas phase)						
B3LYP	EPR-II	1	N(14)	11.58	0.12	0.47
		2	C(13)	-4.14	0.36	-0.02
		7	C(13)	5.20	-0.51	0.02
		15	O(17)	-13.17	-0.38	0.49
		16	C(13)	-5.40	-0.14	-0.02
		17	H(1)	1.33	0.17	0.00
		18	C(13)	5.87	0.30	0.01
		29	C(13)	12.91	-0.05	0.03
		30	O(17)	-0.26	-0.31	0.01
B3LYP	EPR-III	1	N(14)	11.18	-0.10	0.45
		2	C(13)	-4.22	0.35	-0.01
		7	C(13)	5.12	-0.31	0.02
		15	O(17)	-14.35	-0.38	0.50
		16	C(13)	-5.55	0.46	0.01
		17	H(1)	0.92	0.11	0.00
		18	C(13)	6.76	-0.09	-0.01
		29	C(13)	12.22	-0.04	0.02
		30	O(17)	-0.26	-0.41	0.01
POBN-DMF radical (DMF solvent, implicit solvation, SMD model)						
B3LYP	EPR-II	1	N(14)	10.98	0.16	0.49
		2	C(13)	-4.77	0.35	-0.02
		7	C(13)	9.18	-0.55	0.03
		15	O(17)	-13.27	-0.41	0.48
		16	C(13)	-6.51	-0.15	-0.02
		17	H(1)	1.16	0.18	0.00
		18	C(13)	11.32	0.32	0.03
		29	C(13)	6.58	0.01	0.02
		30	O(17)	-0.28	-0.38	0.01
B3LYP	EPR-III	1	N(14)	11.16	0.00	0.46
		2	C(13)	-4.47	0.54	-0.02
		7	C(13)	7.85	-0.51	0.02
		15	O(17)	-14.27	-0.47	0.50
		16	C(13)	-6.22	0.50	0.00
		17	H(1)	1.63	0.16	0.00
		18	C(13)	11.55	-0.18	0.02
		29	C(13)	6.14	-0.07	0.02
		30	O(17)	-0.26	-0.52	0.01

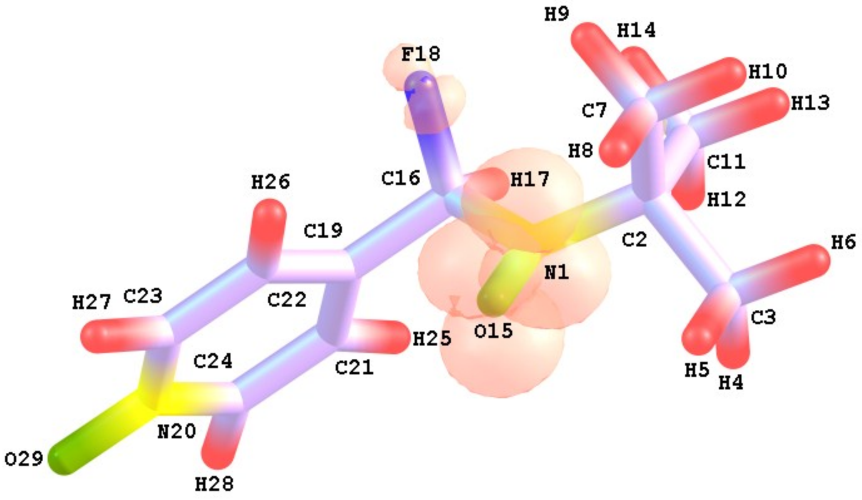

Figure S31 The numbering of atoms and the spin density plot for the optimized structure of a POBN-F radical

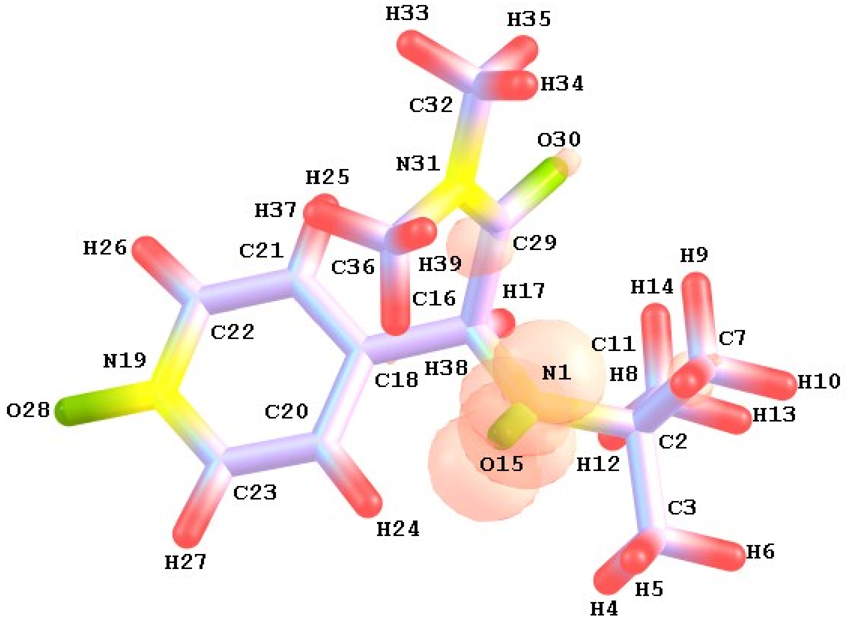

Figure S33 The numbering of atoms and the spin density plot for the optimized structure of a POBN-DMF• radical

References:

(i) Yun, S.M., *et al.*, *Carbon Lett.,* **2007***,* 8, 292-298.

(ii) Tuček, J., *et al.*, *Nat. Commun.* **2017**, 8, 14525.

(iii) Ichihara, J. *et al., Journal of the Chemical Society, Chemical Communications,* **1986**, *10*, 793-794.

(iv) Chai, J.-D., Head-Gordon, M., *Phys. Chem. Chem. Phys.* **2008**, *10*, 6615-6620.

(v) Ditchfield, R; Hehre, W.J; Pople, J. A., *J. Chem. Phys.* **1971**, *54*, 724–728.

(vi) Marenich, A.V.; Cramer, Ch. J.; Truhlar, D. J., *J. Phys. Chem. B*, **2009**, *113*, 6378–6396.

(vii) Frisch, M. J. et al. *Gaussian09.D01*, Gaussian Inc. Wallingford, CT, **2009**.

(viii) Borden, W. T. *Chem. Commun*. **1998**, *18*, 1919-1925.

(ix) Kresse, G., Furthmüller, *J. Phys. Rev. B* **1996**, *54*, 11169–11186.

(x) Klimeš, J., Bowler D. R., Michaelides, A., *Phys. Rev. B* **2011**, *83*, 195131.

(xi) Blöchl, P. E., *Phys. Rev. B* **1994**, *50*, 17953–17979.

(xii) Kresse, G., Joubert, D., *Phys. Rev. B* **1999**, *59*, 1758–1775.

(xiii) Mathew, K., Sundararaman, R., Letchworth-Weaver, K., Arias, T. A., Hennig. R. G., *J. Chem. Phys*. **2014**, *140*, 084106.

(xiv) Wang, X. *et al.*, *Phys. Chem. Chem. Phys.* **2016**, *18*, 3285-3293.

(xv) V. Barone, in Recent Advances in Density Functional Methods, Part I, Ed. D. P. Chong (World Scientific Publ. Co., Singapore, **1996**).